Reconstruction Methods for Level-Crossing Sampling

by

Hsin-Yu Lai

B.S., National Taiwan University (2014)

Submitted to the Department of Electrical Engineering and Computer
Science
in partial fulfillment of the requirements for the degree of

Master of Science in Electrical Engineering and Computer Science

at the

MASSACHUSETTS INSTITUTE OF TECHNOLOGY

June 2016

Author . . . .
Department of Electrical Engineering and Computer Science
May 3, 2016

Certified by . . . .
A. V. Oppenheim
Ford Professor of Engineering
Thesis Supervisor

Accepted by . . . .
Professor Leslie A. Kolodziejski
Chair, Department Committee on Graduate Theses

Reconstruction Methods for Level-Crossing Sampling

by

Hsin-Yu Lai

Submitted to the Department of Electrical Engineering and Computer Science
on May 3, 2016, in partial fulfillment of the
requirements for the degree of
Master of Science in Electrical Engineering and Computer Science

Abstract

Level-crossing sampling refers to a sampling method that generates a sequence of timing samples when a signal crosses a specified set of levels. Conventional sampling techniques more typically rely on producing a sequence of amplitude samples at a specified set of timings. Level-crossing sampling has been considered as a promising alternative to time sampling when it is difficult to implement high-precision quantizers but where high timing resolution is possible. Although Logans theorem provides conditions in which signals are recoverable from samples obtained by zero-crossing, which is a level-crossing sampling method with one level, associated conditions for a multi-level framework have not yet been developed.

This thesis studies a recently proposed level-crossing sampling method, which corresponds to amplitude sampling. This method establishes an amplitude-time relationship representation of the original signal, which is referred to as the amplitude-time function. The pre-designed levels determine when samples of the amplitude-time function are taken. This sampling procedure enables us to design two algorithms, the Bandlimited-Interpolation Approximation (BIA) algorithm and the Iterative Amplitude Sampling Reconstruction (IASR) algorithm, that can reconstruct the original signal from these timing samples with improved accuracy over existing multi-level-crossing sampling approaches. By relating amplitude sampling with nonuniform time sampling, we further compare these algorithms with one of the more efficient nonuniform time sampling methods, the Adaptive Weights Method (AWM). Simulations show that not only do these two algorithms attain high signal-to-error ratio (SER), but the IASR can generally reconstruct the original signal with fewer iterations than the AWM.

Thesis Supervisor: A. V. Oppenheim
Title: Ford Professor of Engineering

Acknowledgments

I would like to first thank my research advisor Professor Alan Oppenheim for remarkable guidance for this thesis in several ways. To begin with, he has provided me with lots of insights, which offered me different angles in my research. Moreover, he has taught me how to express ideas more efficiently. I remembered when we discussed the iterative amplitude sampling reconstruction algorithm, Al immediately asked me to draw a flow diagram, from which people should be able to understand the algorithm. He has also improved my English writing a lot. For example, he has taught me to consider my target readers and to imagine their reactions when I was writing. I am also extremely grateful for having him as my mentor. He gave me challenges to help me eliminate my weakness, such as encouraging me to present in our weekly group meeting and to hold a poster session so that I can learn to be more aggressive. Besides these challenges, he also gave me belief in accomplishing great research. With the gain of confidence, I was not afraid of any difficulty and was always eager to spend more time in my research. He has also given me a great number of suggestions in internship, classes, and attitudes. With all of these, I gained my knowledge in both practice and theory, and also learned to be more and more mature.

I'd also like to express my deep thanks to all my labmates. I'd like to thank my extremely acknowledged collaborator, Pablo, for sharing lots of knowledge and bringing me so many wonderful discussions. He also brought me lots of joy in my daily life and has always lighten me up. I really cannot thank Guolong more, who has offered me innumerable help in literally everything: cultural difference, tax and OPT, English, finding jobs, classes, and research. Because of Guolong, I am not afraid of any challenge since I know there is someone who is so brilliant and unselfishness that will be there advising me, and Guolong himself is the model who proves that there is no real obstacle. I also want to thank Tarek, who in my viewpoint, is so mature, creative, sharp, and caring. He not only shares with me lots of insightful thoughts in research, such as his understanding in optimization and algebra, but also shares with me lots of invaluable suggestions in life, such as how to write papers and communicate

with thesis committees. I'd like to thank my officemate Catherine as well. Although we just started sharing the same office from this semester, I've already received so much warmness from her. I remembered her warm little notes, her ginger tea, her support in my poster session, and most importantly all the sincere companion.

I also want to thank all the attendees for DSPG weekly group meeting. I especially want to thank Petros since it is his idea to think about iterations on the functional composition formulation of the definition of the amplitude-time function, which inspired me to think of an iterative algorithm for implementing the amplitude-time transformation m_α. I want to thank Tom. He was always so ecstatic in each group meeting discussion and always threw out so many amazing ideas. I really admire his deep understanding in signal processing and his craving in knowledge. I want to thank Jennifer and Austin, especially Austin, for trying to help me with my research and being supportive friends. I also want to thank Jim for being so caring. I also want to thank Sefa, Dan, and a recent visitor from DSPG alumni, Meir, for providing ideas about my future research direction. Moreover, I want to thank Laura, Yugandi, Leslie for all the administrative support; Yugandi, in particular, has also supported me a lot in life as a nice friend. I also want to thank Arthur and Elaina for an unforgettable summer.

Most importantly, I want to thank my family, my mother particularly, as my mental support. I have been through so many difficulties since I came here as an international student whose native language is not English, and was used to a more conservative culture that values more on humbleness rather than confidence. However, because of my family, I know I have a shoulder to cry on and I know even if I fail, my family will still be there to comfort me and help me to start over again. With my parents, I can walk through these difficulties and keep learning precious experience from them. I want to thank my mother for our weekly two-hour long skype talk (both of us are reluctant to hang off), thank my deer brother for bringing me so much joy (I believe my brother's brain is shaped differently since he always can think of some weird and brilliant ideas), and my father, who although is busy, cares a lot about whether I live well here. I love you all. With you, I cannot be a happier person.

Contents

List of Figures

Chapter 1

Introduction

1.1 Motivation

Sampling theorems play an important role in signal processing as a connection between the analog world and digital processing. The most well-studied sampling theorem is the Shannon-Nyquist theorem [1], which formalizes a discrete representation of a bandlimited signal. It has had a profound impact on communication systems, the digital signal processing industry, and a great number of extensions have been proposed [2–4]. However, the Shannon-Nyquist sampling theorem and most of its extensions study a time-sampling framework, where a signal is represented by a continuous amplitude sequence corresponding to a specified set of time values. When a high-precision quantizer is difficult to implement but timing resolution can be sufficiently high, a promising alternative to the time-sampling method is level-crossing sampling [5], in which the time values are recorded when the signal crosses a specified set of thresholds. Therefore, a signal is instead represented by a time sequence and its amplitude information is inherited in the sampling methodology.

A significant result of level-crossing sampling is Logan's theorem [6], which studies a specific class of level-crossing sampling – zero-crossing sampling, in which the level is set to be zero. The theorem provides sufficient conditions for reconstructing a signal under zero-crossing sampling. In [7], Petros showed that although Logan's theorem

provides no stability[1] guarantee, stability can typically be ensured with additional assumptions on the sparsity of some basis. However, a more generalized theorem for level-crossing sampling with multiple levels is still not discovered. Most existing generalized level-crossing sampling methods focus on a low-power-consumption Analog-to-Digital Converter design [8–10]. They simply reconstruct signals by the zero-order-hold and thus represent piecewise-constant approximations of the original signal. Advanced signal reconstruction techniques for generalized level-crossing sampling are still under-explored.

This thesis studies a framework, referred to as amplitude sampling, recently proposed in ongoing doctoral research described in [11]. This framework potentially allows us to theoretically pursue a more accurate reconstruction than most existing level-crossing sampling methods with multiple levels. Specifically, while conventional level-crossing sampling methods only consider samples as amplitude-time ordered pairs and therefore lose information in between, amplitude sampling establishes an amplitude-time representation of the entire signal. It is accomplished first by adding a ramp to the signal to make it strictly monotonic and then using the monotonic function as the one-to-one mapping between time and amplitude. With the mapping, a function expressed in an amplitude-time relationship can be achieved, which we will later refer to as the amplitude-time function. Samples taken from amplitude-time functions form a time sequence. Therefore as conventional level-crossing sampling techniques, amplitude sampling represents the original signal by a time sequence. Our goal is to recover the original signal from this sequence.

The thesis focuses on establishing algorithms to reconstruct a bandlimited signal from uniform samples of its corresponding amplitude-time function. The bandlimited assumption will be utilized to design amplitude sampling reconstructions. This assumption can be more generalized in future study. With the bandlimited assumption, there is an additional advantage to using amplitude sampling over level-crossing sampling. We know that if an input signal f is bandlimited and has finite energy, i.e. $f \in L_2$, it attenuates to zero as time goes to infinity. Therefore, it will stop crossing

---

[1]The definition of stability will be given in Chapter 2

predefined levels after a finite amount of time under a level-sampling regime. Without any further assumption other than the bandlimitedness, these obtained samples cannot be a sampling sequence[2] and cannot be able to reconstruct the original function in practice. However, in amplitude sampling, the slope of the ramp can be carefully chosen so that the density of the samples in time can be guaranteed to satisfy the nonuniform sampling theorem for a stable reconstruction. Therefore, the error of a resulting bandlimited function from an amplitude sampling reconstruction algorithm can be bounded by a finite scaling of the error on the sufficiently dense samples. In this thesis, samples on amplitude-time functions are uniformly taken since uniform levels are easy to implement. This also can potentially be generalized in future work.

To reconstruct the original signal from amplitude sampling, two steps are needed; the first step is to realize the transformation between the amplitude-time function and the original signal, and the second step is to approximate a continuous signal from discrete samples in amplitude. An iterative algorithm is proposed for the first step to attain the transformation, with which two other algorithms, the bandlimited-interpolation approximation (BIA) and the iterative amplitude sampling reconstruction (IASR), are introduced for the second step. The BIA is a direct approximate algorithm that can achieve arbitrarily large signal-to-error ratio (SER) by increasing the sampling rate; the IASR on the other hand is an iterative algorithm that may be able to converge to the original function when the sampling density is sufficiently high.

Since uniform samples in amplitude can be one-to-one mapped to nonuniform samples in time, another way to reconstruct the original signal is to recover the signal from these nonuniform samples by nonuniform time sampling reconstruction methods. Background study on nonuniform time sampling theorem and algorithms is provided in Section 2.1. In this thesis, simulations based on different parameter settings are performed to compare our proposed algorithms with a specific nonuniform sampling method, the adaptive weights method (AWM), which is proven to be the most efficient algorithm in numerical experiments [12]. Since our proposed algorithms are designed

---

[2]The definition of a sampling sequence will be provided in Section 2.1

based on amplitude sampling, the SER of both the BIA and the IASR after the first iteration is significantly greater than that of the AWM after the first iteration. In most simulation results, the IASR converges within fewer iterations than the AWM. Moreover, simulation results suggest two major differences between parameter effects on the convergence rate of the IASR and of the AWM. We show that with those two differences, parameters can be designed to further improve the convergence rate of the IASR.

The remaining of the thesis is organized as follows. Section 1.2 provides the definition of amplitude-time functions and formulates the amplitude sampling regime. Chapter 2 studies backgrounds for nonuniform sampling theorems, iterative nonuniform sampling algorithms, and specifically the AWM. Chapter 3 explores time-domain properties of amplitude-time functions. These properties include the periodicity of amplitude-time functions when input signals are periodic and properties that result from two interpretations of the transformation m_α: a matrix representation and an interpretation that can be indicated in a figure. These two interpretations will be introduced in Chapter 3. Moreover, with the figurative interpretation, we also develop and prove an iterative algorithm that realizes the transformation between time-amplitude functions and amplitude-time functions. With this realization, in amplitude sampling reconstruction design we can assume that the transformation is implementable. Chapter 4 discusses frequency-domain properties of amplitude-time functions, which are useful both in designing amplitude sampling reconstruction algorithms and in performance analysis of these algorithms. Chapter 5 proposes two amplitude sampling algorithms, the BIA and the IASR, to reconstruct the original signal. Simulation settings and results are discussed in details and how parameters can be chosen to be beneficial for amplitude sampling reconstruction is suggested. Chapter 6 concludes the thesis and outlines some future research directions.

1.2 Problem Definition

In this section, we provide the definition of amplitude-time functions, which as mentioned in Section 1.1 is a representation of the original signal $f(t)$ in an amplitude-time relationship derived by a one-to-one mapping between time and amplitude. Recall that the signal $f(t)$ is assumed to be bandlimited. By Bernstein's inequality [13], if a function is bandlimited, its first derivative is bounded. Therefore, a simple method to obtain a strictly monotonic function as the one-to-one mapping between time and amplitude is to add a ramp with a sufficiently high slope αt to $f(t)$, i.e. the acquired monotonic function $g(t) = f(t) + \alpha t = y$ satisfies $g'(t) = f'(t) + \alpha > 0$, where y can be thought of as the amplitude variable. Then the corresponding amplitude-time function $h(y)$ can be defined as

$$h(y) = g^{-1}(y) - \frac{1}{\alpha}y. \tag{1.1}$$

Under such a definition, $h(y)$ with $y = f(t) + \alpha t$ is bounded if $f(t)$ is bounded since

$$h(f(t) + \alpha t) = t - \frac{1}{\alpha}(f(t) + \alpha t)$$
$$= -\frac{1}{\alpha}f(t). \tag{1.2}$$

From (1.2), we obtain a relationship between f and h in the form of functional composition [14]. Moreover, since $g(t) = f(t) + \alpha t$ is designed to be invertible, this relationship uniquely determines h from f.

A similar procedure is used to express $f(t)$ in terms of $h(y)$. The slope of the ramp is selected to be $1/\alpha$ so that the inverse function of $t = h(y) + y/\alpha$ is $g(t)$. Note that y/α is sufficiently large, i.e. $h'(y) + 1/\alpha > 0$. After αt is subtracted from $g(t)$, $f(t)$ is recovered. Therefore another relationship between f and h can be formulated as

$$f(h(y) + \frac{1}{\alpha}y) = -\alpha h(y). \tag{1.3}$$

A similar argument can be made to show that Eq. (1.3) uniquely determines f

$$f \longrightarrow \boxed{m_\alpha} \longrightarrow h \qquad\qquad h \longrightarrow \boxed{m_{\frac{1}{\alpha}}} \longrightarrow f$$

Figure 1-1: The transformation m_α uniquely determines h from f as defined in Eq. (1.2). Similarly, the reconstruction of f from h is $m_{1/\alpha}$ as shown in Eq. (1.3).

from h. In summary, as shown in Figure 1-1, the relationships in (1.2) and (1.3) can be interpreted as an invertible transformation between f and h. The subscript α of the transformation m_α is the slope of the corresponding ramp. As we will see in Section 3.4, the relationships in Figure 1-1 is useful in designing algorithms to attain h from f (or f from h) since it may not be feasible to directly implement an inverse function. With the definition of amplitude-time functions and the m_α transformation, we now can explore how to recover a signal from uniform samples of its corresponding amplitude-time function.

Chapter 2

Nonuniform Time Sampling: A Short Review

Since the early work on the Shannon-Nyquist theorem, many extensions have been introduced such as sampling theorems for bandpass signals, sampling theorems for time-limited signals [1], and sampling with the value of a signal and its derivatives [15], [16]. In this chapter, we focus on nonuniform sampling. As mentioned in Chapter 1, in amplitude sampling, uniform samples $\{h(n\Delta)\}$ of the amplitude-time function can be mapped to nonuniform samples $\{f(t_n)\}$ of the original signal. Nonuniform sampling theorems provide a basis for analyzing the accuracy of our proposed reconstruction algorithms. Moreover, once nonuniform samples are obtained, nonuniform sampling methods can be applied to recover $f(t)$. Therefore, we can evaluate the efficiency of our proposed algorithms by comparing our methods with nonuniform sampling reconstruction methods. Both aspects will be explored in Chapter 5.

We provide background for nonuniform sampling of bandlimited signals in this chapter [2]. Definitions and conditions for a sequence of nonuniform samples to be a uniqueness sequence and a sampling sequence are first presented. We will show in Section 2.1 how these definitions relate to the validity of nonuniform sampling methods. Several nonuniform sampling methods are then discussed. Moreover, since we

---
[1]Time-limited signals refer to signals $f(t)$ that are 0 when $|t| > T$ for some T.
[2]We mention in Section 1.1 that we focus on recovering bandlimited signals and the reason why such constraint is reasonable is also discussed in Section 1.1.

propose an iterative reconstruction algorithm for amplitude sampling, a general structure of iterative nonuniform sampling reconstruction is demonstrated as a basis for comparing our algorithm with this structure. Among iterative nonuniform sampling algorithms, we describe the adaptive weights method (AWM) in the most details. This method has been shown to perform the best in numerical results [12]. Thus, we later compare our proposed iterative reconstruction algorithm with the AWM in Section 5.4.

2.1　The Nonuniform Sampling Theorem

As mentioned earlier, definitions of a uniqueness sequence and a sampling sequence will be presented. A uniqueness sequence is defined as follows:

Definition 2.1. [17, 18] *The set of points $\{t_n\}$ is a uniqueness sequence for $\mathcal{B}(S)$ if there are no two different functions $f, g \in \mathcal{B}(S)$ that agree in $\{t_n\}$.*

Here we can take $\mathcal{B}(S)$ as the space of bandlimited signals with S as its support in frequency domain. It is clear that if there exist two different bandlimited functions f and g that agree in $\{t_n\}$, then we cannot distinguish $\{g(t_n)\}$ from $\{f(t_n)\}$ and therefore we cannot reconstruct both f and g based on these samples with merely the bandlimited assumption. That is, $\{f(t_n)\}$ can be a representation of $f(t)$ in $\mathcal{B}(S)$ if and only if $\{t_n\}$ is a uniqueness sequence.

The idea of representing a signal by its nonuniform sampling can be traced back to Cauchy as stated in Black's paper [19]. Black also discussed scenarios where nonuniform sampling is encountered, for example, random sampling for nonsynchronous multiplexing [19]. They stated possible conditions for a uniqueness sequence for a bandlimited-signal space. These conditions were later proved by [20, 21] in the following theorem:

Theorem 2.2. [20] *If the average sampling rate of the nonuniform samples $(t_n, f(t_n))$ is higher than the Nyquist rate, the nonuniform samples can uniquely represent a bandlimited signal. That is, $\{t_n\}$ is a uniqueness sequence for $\mathcal{B}(S)$ being the bandlimited signal space.*

A more rigorous statement can be found in [21], in which Beutler also proved the theorem but in a more general mathematical setting.

However, Theorem 2.2 is not useful in practice since it does not imply how a finite-energy perturbation on samples affects the reconstructed signal. The resulting error can be unbounded. In reality we can hardly design an algorithm with infinite precision or introduce no measure error. The definition of a sampling sequence was then introduced to resolve this issue as shown in the follows:

Definition 2.3. [17] *The set of points $\{t_n\}$ is a sampling sequence for $\mathcal{B}(S)$ if there exists a constant K such that*

$$\int_{-\infty}^{\infty} \|f(t)\|^2 dt \leq K \sum \|f(t_n)\|^2 \tag{2.1}$$

for all $f(t) \in \mathcal{B}(S)$, where $\mathcal{B}(S)$ consists of all square integrable function whose Fourier transform is supported on S.

We first notice that Definition 2.3 implies $\{t_n\}$ is also a uniqueness sequence but the converse does not hold. Definition 2.3 ensures that the error induced by noisy samples will be bounded if the noise is also bounded; sampling with a sampling sequence is known as stable sampling. In order to be able to present the conditions for a sampling sequence, the definition of the Beurling lower density is given as follows:

Definition 2.4. [22, 23] *The Beurling lower density of a sequence $\{t_n\}$ is defined as*

$$D_-(\{t_n\}) = \liminf_{r \to \infty} \inf_a \frac{1}{r} \sharp\{\{t_n\} \cap [a, a+r]\}. \tag{2.2}$$

We now can state the necessary and sufficient conditions for a sampling sequence in the following theorem that was proved in [17] :

Theorem 2.5. [17] *A sequence $\{t_n\}$ is a set of stable sampling for $\mathcal{B}(S)$ if the Beurling lower density $D_-(\{t_n\})$ is at least $\frac{m(S)}{2\pi}$, where $m(S)$ is the measurement of the support of S.*

19

In cases where there are infinite samples in the past or within a finite interval, since such samples constitute a uniqueness sequence but not a sampling sequence, a small perturbation can lead to a greatly different reconstructed signal.

From Theorem 2.2 and 2.5, if the Beurling lower density is higher than the Nyquist rate, uniqueness is ensured and stable reconstruction is possible. Several reconstruction methods have been proposed under this condition. Yen [4] considered three nonuniform sampling regimes: migrations of a finite number of uniform samples, uniform samples with a single gap, and recurrent nonuniform sampling. The last sampling regime gives an explicit formula to reconstruct a signal from groups of N points where each group satisfies Theorem 2.2. However, Yen's method is impractical to realize [24]. Yao and Thomas derived a Langrange interpolation formula as a representation for samples deviating from its uniform counterpart by less than $(1/4)$ unit [25]. They showed in a later paper [26] that the reconstruction is not stable when some samples deviate more than $(1/4)$ unit. Yao and Thomas discovered that a Lagrange interpolation representation guarantees the stability.

Besides directly reconstructing signals by taking interpolations on nonuniform samples, an alternative is iterative reconstruction, which has been shown to be more applicable in practice. In [20], applications of nonuniform sampling reconstruction such as video coding and error concealment are shown. Several iterative reconstruction methods have been discussed [12], many of which follow a structure that will be described in the next section. Moreover, a highly practical iterative reconstruction method, the adaptive weights method, will be stated in Section 2.2 and will later be compared with the algorithms developed in this thesis.

2.2 Iterative Nonuniform Sampling Reconstructions and the Adaptive Weigths Method (AWM)

In this section, we provide more details on iterative nonuniform sampling reconstruction not only because it is usually more practical than direct reconstruction but also

because we later use it to evaluate the performance of our proposed iterative ampli-
tude sampling algorithm. This section first presents a general technique for developing
an iterative reconstruction algorithm, where we follow the discussion in [12]. Then we
will focus on one particular algorithm, the adaptive weights method (AWM), showing
how it utilizes the technique and giving the bound for its convergence rate. The AWM
then will be used to compare our proposed algorithms.

We first state a proposition presented in [12]:

Proposition 2.6. **[12]** *Let A be a bounded operator on a Banach space $(B, \|\cdot\|_B)$*
such that there exists some $\gamma < 1$

$$\|f - Af\|_B \leq \gamma \|f\|_B, \tag{2.3}$$

for all f in B. Then A is invertible on B and f can be recovered from Af by the
following iteration algorithm. Setting $f_0 = 0$ and

$$f_{n+1} = f_n + A(f - f_n), \tag{2.4}$$

we have $\lim_{n \to \infty} f_n = f$ and

$$\|f - f_n\|_B \leq \gamma^{n+1} \|f\|_B. \tag{2.5}$$

We note that the linear convergence shown in Eq. (2.5) can be observed by
rewriting Eq. (2.4) as $f - f_{n+1} = f - f_n - A(f - f_n) = (Id - A)(f - f_n)$. Since from Eq.
(2.3), we know $\|I - A\| \leq \gamma$, we therefore obtain $\|f - f_{n+1}\|_B = \|(Id - A)(f - f_n)\|_B <$
$\gamma \|f - f_n\|_B$. By Banach fixed point theorem [27], we have $\lim_{n \to \infty} f_n = f$ and
$\|f - f_n\|_B \leq \gamma^{n+1} \|f - f_0\|_B$ which is exactly Eq. (2.5).

The strategy of Proposition 2.6 has been applied in a number of nonuniform
sampling algorithms [28, 29]. Due to the linearity in Eq. (2.4), once the operator A
is found and a parameter $\gamma < 1$ is found to satisfy Eq. (2.3), this strategy is easy
to be implemented; moreover, it guarantees a geometric convergence rate. In order

to find a class of sampling spaces that are applicable to this proposition, [12] focused on the study of frames. [12] indicated that if a sequence of frames can be discovered, then A can be defined as the frame operator [3] and can be proved to satisfy Eq. (2.3). Furthermore, the convergence rate and the stability can be determined by the upper and lower frame bounds. Among these frame methods, the AWM was shown to be practical due to its simplicity, fast convergence rate, and robustness compared to several other iterative methods [12]. It is especially beneficial in a numerical aspect since the interpolation function of the AWM is of finite-length support, which can be numerically realized without introducing errors. As a result, we later compare our iterative amplitude sampling reconstruction (IASR) algorithm with the AWM. The AWM algorithm is as follows:

Assume that there is a nonuniform sequence of timing $\ldots < t_n < t_{n+1} < \ldots$ at which samples are obtained. We denote χ_n as the characteristic function of half interval $[t_n, t_{n+1})$; i.e. $\chi_n(t) = 1$ if $t \in [t_n, t_{n+1})$ and zero otherwise. We then obtain a zero order hold approximation of f by $\sum_{n \in \mathbb{N}} f(t_n)\chi_n(t)$. The operator A is defined as passing the zero order hold approximation through a low-pass filter with the cutoff frequency as the bandwidth of f. That is, $Af = P(\sum_{n \in \mathbb{N}} f(t_n)\chi_n(t))$ where the operator P represents the low-pass filter. With the operator A, now we can state the following theorem.

Theorem 2.7. **[12]** *If $\delta = \sup(t_{n+1} - t_n) < \frac{\pi}{W}$ where W is the bandwidth of $f(t)$, then f is uniquely determined by its samples $f(t_n)$ and can be reconstructed iteratively as follows:*

$$f_0 = Af = P(\sum_{n \in \mathbb{N}} f(t_n)\chi_n(t)).f_{k+1} = f_k + A(f - f_k). \tag{2.6}$$

Then $\lim_{n \to \infty} f_n = f$ and

$$\|f - f_k\|_B \leq (\frac{\delta W}{\pi})^{k+1}\|f\|_B. \tag{2.7}$$

---

[3]Both the definition of frames and the way to relate A with a frame operator can be found in [12].
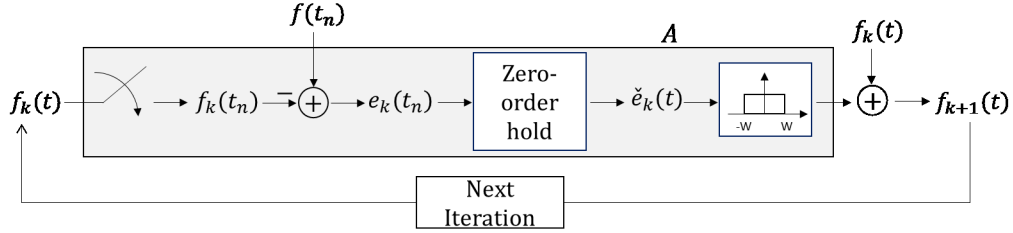
Figure 2-1: Adaptive weights method (AWM) in amplitude sampling reconstruction where k denotes the index of iterations

This theorem shows the AWM converges linearly with the convergence rate $r = \frac{\delta W}{\pi}$ [4]. The proof of this theorem can be found in [12]. We should notice that the convergence rate is determined by the maximum time difference δ and the bandwidth W. Since δ is not the Beurling lower sampling density (or the average sampling rate in generic cases), it is more restrictive than the requirement for a unique and stable sequence as in Theorem 2.5. In fact, when we apply the AWM to amplitude sampling, δ is affected by the transformation parameter α and the first derivative of the original signal f. It will be clarified further in Section 5.4 when the AWM is compared with our proposed algorithms. Here we first give a flow diagram Figure 2-1 to explain how the AWM can fit into amplitude sampling settings.

As indicated in Figure 2-1, the uniform samples $\{(n\Delta, h(n\Delta))\}$ of an amplitude-time function are first mapped to the corresponding nonuniform sampling points $\{(t_n, f(t_n))\}$ on the original signal. Then the AWM is applied to these nonuniform samples. Figure 2-1 will be revisited in Chapter 5.

---

[4]The convergence rate r of a sequence $\{x_k\}$ with linear convergence is defined to be $\lim_{k\to\infty} \frac{\|x_{k+1}-x^*\|}{\|x_k-x^*\|}$ where $\lim_{k\to\infty} = x^*$. Therefore, the sequence converges faster as the convergence rate $r \to 0$.

Chapter 3

Time Domain Properties of Amplitude-time Functions

In this chapter, we study the relationship between f and h in the time domain. In Chapter 4, we will discuss the relationship in the frequency domain. Exploring properties of the relationship is helpful for understanding the nature of amplitude sampling and for developing reconstruction algorithms. However, since the transformation m_α on $f(t)$ is not linear, i.e. $m_\alpha(f_1 + f_2) \neq m_\alpha(f_1) + m_\alpha(f_2)$, even if f can be expressed as a linear combination of some simple functions, h may not be able to have an explicit formulation related to the linear combination. Therefore, it is generally difficult to analyze whether properties such as periodicity and bandlimitedness of time-amplitude functions can be preserved in their corresponding amplitude-time functions. Nevertheless, this analysis is important since it provides insights in reconstruction algorithm design and is crucial for reconstruction error analysis. Periodicity in particular will be studied in this chapter and bandlimitedness will be explored in Chapter 4; these properties will be revisited in Chapter 5 when we discuss amplitude sampling reconstruction design.

To better understand the transformation m_α, we provide two interpretations; one is a matrix formulation and the other is a figurative expression. While the matrix formulation is important for analyzing parameter effects on amplitude sampling reconstruction algorithms in Section 5.4, the figurative interpretation illustrates an

iterative algorithm to realize the transformation m_α, which may be difficult to directly realize by its original definition: obtaining the inverse function of the function $g(t) = f(t) + \alpha t = y$ and subtracting the inverse function with a ramp $\frac{1}{\alpha}y$. The iterative algorithm and its convergence rate are stated in Section 3.4. With the algorithm, we can then assume that the transformation m_α is implementable and can be inherited in our reconstruction algorithms for f from uniform samples of h as developed in Chapter 5.

3.1 Properties of m_α for Periodic Signals

In this section, we demonstrate that periodicity is preserved under the transformation m_α.

If $f(t)$ is periodic with a period T, i.e.

$$f(t + T) = f(t), \tag{3.1}$$

then the following can be obtained:

$$\begin{aligned} g(t + T) &= f(t + T) + \alpha(t + T) \\ &= f(t) + \alpha(t + T) \\ &= y + \alpha T, \end{aligned} \tag{3.2}$$

where $g(t) = f(t) + \alpha t = y$, and thus

$$t + T = g^{-1}(y + \alpha T). \tag{3.3}$$

From Eq. (3.3), $h(y)$ is periodic with period αT:

$$\begin{aligned}
h(y + \alpha T) &= g^{-1}(y + \alpha T) - \frac{1}{\alpha}(y + \alpha T) \\
&= t + T - \frac{1}{\alpha}(y + \alpha T) \\
&= g^{-1}(y) - \frac{1}{\alpha}y \\
&= h(y).
\end{aligned} \qquad (3.4)$$

Therefore periodicity is preserved under the transformation m_α and if $f(t)$ is periodic with a period T, then $h(y)$ is periodic with a period αT. The study of periodic input signals is important for several reasons. Recall that our goal is to design a reconstruction algorithm for amplitude sampling on bandlimited signals. If the input signals are both bandlimited and periodic, then they will only consist of finite number of harmonics. With this simplification, it might be possible to analyze how the number and the size of these harmonics correspond to harmonics in $h(y)$. Moreover, to compute the Fourier transform, we only need to take a finite number of samples and calculate their discrete Fourier transform (DFT) coefficients. For periodic and bandlimited functions, the DFT of samples of one period will not introduce aliasing or resolution issues. Moreover, since h is also periodic when f is periodic, as we will show in Section 5.3.3, we can simulate bandlimited interpolation of uniform samples $h(n\Delta)$ without any truncation error [1]. Understanding periodic functions will therefore be helpful for evaluating our simulation results.

3.2 Matrix Representation of m_α

As mentioned in the beginning of this chapter, we introduce a matrix representation and figurative interpretation of m_α. The matrix representation will be provided in this section along with properties that will be derived from this representation.

As motivation for the matrix formulation of m_α, we discuss the following. Al-

---

[1]The truncation error refers to the error that is induced by approximating bandlimited-interpolation by a sum of finite number of truncated sinc functions. It will be made more clear in Section 5.3.3

though we have shown in Section 3.1 that periodicity can be preserved under the transformation m_α and this may lead to an approachable simplification for our reconstruction problem, it is still not clear whether a bandlimited periodic function can be reconstructed. Since a bandlimited periodic function consists of a finite number of harmonics, understanding how these harmonics interact with each other under the transformation may be helpful to understand the corresponding amplitude-time function. For example, we would like to find the relationship between $m_\alpha(\sin t)$ and $m_\alpha(\sin 2t)$, between $m_\alpha(\sin t)$ and $m_\alpha(2\sin t)$, and between $m_\alpha(\sin t)$ and $m_{2\alpha}(\sin t)$. That is, how time scaling, amplitude scaling, and a change of α affect the associated amplitude-time function. Interestingly, the answer to this question can be easily derived once we express m_α in a matrix form.

In the following subsections, we first define scaled amplitude-time functions $\tilde{h}$, redefine the corresponding transformation based on the relationship between f and $\tilde{h}$, and show the matrix representation of the scaled transformation $\tilde{m}_\alpha$. We then utilize this matrix representation to help us study the relationships we mention in the last paragraph.

3.2.1 Scaled Amplitude-time Functions and Matrix Representation of $\tilde{m}_\alpha$

We now introduce the definition of scaled amplitude-time functions and the corresponding scaled transformation $\tilde{m}_\alpha$. As shown in Eq. (1.2) and Eq. (1.3), the parameter α can be viewed as a scaling factor both in amplitude and time, since the factor $-\frac{1}{\alpha}$ multiplies $f(t)$ and the factor α scales the variable t in the warped function of h. Therefore, when f is fixed but α increases, the corresponding function h shrinks in amplitude but expands in time. This effect can also be observed from Section 3.1, where scaling the period with α implies an expansion in time. To normalize for these effects, we define the scaled amplitude-time function as

$$\tilde{h}(y) = -\alpha h(\alpha y). \tag{3.5}$$

28
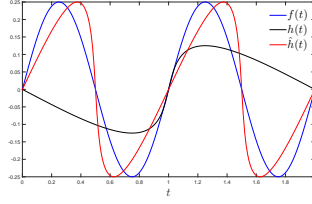
Figure 3-1: Figures of f, h, $\tilde{h}$

From Eq. (3.5), a new relationship between $f(t)$ and $\tilde{h}(y)$ which we denote by $\tilde{m}_\alpha$ can be expressed as

$$f(y - \frac{1}{\alpha}\tilde{h}(y)) = \tilde{h}(y).$$
$$\tilde{h}(t + \frac{1}{\alpha}f(t)) = f(t). \tag{3.6}$$

Since in this subsection we will discuss how time scaling, amplitude scaling, and a change of α affect the corresponding amplitude-time function, we add subscripts to each (scaled) amplitude-time function to avoid ambiguity. That is, $h_{\alpha,f}(y)$ stands for $m_\alpha(f)(y)$ and $\tilde{h}_{\alpha,f}(y)$ stands for $\tilde{m}_\alpha(f)(y)$.

After h is normalized as in Eq. (3.5), the relationship of the corresponding parameter α between a transformation from f to $\tilde{h}$ and the transformation from $\tilde{h}$ back to f differs in signs rather than being reciprocals to each other. Moreover, from Eq. (3.6), both scaling factors that are previously in front of $\tilde{h}$ and in front of the t in the warped function of f in Eq. (1.2) no longer exist. If $\tilde{h}$ and f are drawn in the same figure, as shown in Figure 3-1, $\tilde{h}$ can be interpreted as a tilted f. Furthermore, from Eq. (3.6), as α goes to infinity, $\tilde{h}(t)$ will become $f(t)$. Since $\tilde{h}$ is the scaled replica of h, as $\tilde{h}$ approaches the bandlimited function f, h intuitively will be more and more similar to a bandlimited function. This intuition will be strengthened by properties of the Fourier transform of h as presented in Chapter 4.

The relationships in Eq. (3.6) can also be expressed in a matrix formulation as

$$\begin{bmatrix} y \\ \tilde{h}_{\alpha,f}(y) \end{bmatrix} = \begin{bmatrix} 1 & \frac{1}{\alpha} \\ 0 & 1 \end{bmatrix} \begin{bmatrix} t \\ f(t) \end{bmatrix}. \tag{3.7}$$

Note that because of the scaling, the matrix has unit diagonal entries. Along

with the fact that the matrix is uppertriangular, the matrix representation of the transformation $\tilde{m}_\alpha$ forms the unitriangular group. This fact indicates the invertibility, commutability, and transitivity of the transformation. Moreover, the matrix form indicates that although the transformation between f and $\tilde{h}$ is not linear, the transformation between $(t, f(t))$ and $(y, \tilde{h}(y))$ is. This matrix interpretation leads to the observations of the following two properties described in the next two subsections respectively.

3.2.2 Time Scaling and Amplitude Scaling Effects on Scaled Amplitude-time Functions

In this subsection we explain how time scaling and amplitude scaling on f affect $\tilde{h}$. We first interpret time scaling and amplitude scaling on $f(t)$ in a matrix form. The scaled function $\tilde{f}(t) = Af(t/B)$ can be expressed as

$$\begin{bmatrix} \tilde{t} \\ \tilde{f}(\tilde{t}) \end{bmatrix} = \begin{bmatrix} B & 0 \\ 0 & A \end{bmatrix} \begin{bmatrix} t \\ f(t) \end{bmatrix}. \tag{3.8}$$

As a result, we could express the procedure of operating on $\tilde{f}(t)$ with $\tilde{m}_\alpha$ to obtain $\tilde{h}_{\alpha,\tilde{f}}(y)$ as

$$\begin{bmatrix} \tilde{y} \\ \tilde{h}_{\alpha,\tilde{f}}(\tilde{y}) \end{bmatrix} = \begin{bmatrix} 1 & \frac{1}{\alpha} \\ 0 & 1 \end{bmatrix} \begin{bmatrix} B & 0 \\ 0 & A \end{bmatrix} \begin{bmatrix} t \\ f(t) \end{bmatrix} = \begin{bmatrix} B & 0 \\ 0 & A \end{bmatrix} \begin{bmatrix} 1 & \frac{A}{B\alpha} \\ 0 & 1 \end{bmatrix} \begin{bmatrix} t \\ f(t) \end{bmatrix} = \begin{bmatrix} B & 0 \\ 0 & A \end{bmatrix} \begin{bmatrix} y \\ \tilde{h}_{B\alpha/A,f}(y) \end{bmatrix}. \tag{3.9}$$

The matrix formulation in Eq. (3.9) can also be expressed as:

$$\tilde{y} = By.$$
$$\tilde{h}_{\alpha,\tilde{f}}(\tilde{y}) = \tilde{h}_{B\alpha/A,f}(y). \tag{3.10}$$

The equations (3.5) and (3.10) lead to:

$$\tilde{h}_{\alpha,\tilde{f}}(y) = \tilde{h}_{B\alpha/A,f}(\frac{y}{B}).$$

$$\Rightarrow -\alpha h_{\alpha,\tilde{f}}(\alpha y) = -\frac{B\alpha}{A}h_{B\alpha/A,f}(\frac{B\alpha}{A}\frac{y}{B}) = -\frac{B\alpha}{A}h_{B\alpha/A,f}(\frac{\alpha y}{A}). \qquad (3.11)$$

As a result, the amplitude-time function obtained from a scaled f can also be attained by scaling an amplitude-time function which is transformed from the unscaled f but with a scaled α. In fact, when $A = 1$, Eq. (3.11) becomes

$$h_{\alpha,\tilde{f}}(y) = Bh_{B\alpha,f}(y); \qquad (3.12)$$

when $A = B$, Eq. (3.11) becomes

$$h_{\alpha,\tilde{f}}(y) = h_{\alpha,f}(y/A). \qquad (3.13)$$

From Eq. (3.12) we observe that functions related by time-scaling correspond to the same amplitude-time function with corresponding amplitude-scaling when the transformation m_α is chosen according to the scaling factor. This leads to an interesting discussion about how our reconstruction algorithm performs when it is dealing with the same amplitude-time function but is trying to reconstruct f with different bandwidths.

From Eq. (3.13), we observe that when the ratio of the amplitude scaling factor A to the time expanding factor B is fixed, the corresponding amplitude-time function will be the same except that its timing will be scaled correspondingly with A. It suggests the Fourier transform of the amplitude-time function corresponding to $f(At)$ will be that corresponding to $Af(t)$ with expanding frequency. Discussions on this effect will be provided in Section 5.4.2.2 and 5.4.2.3. This observation is also important for amplitude sampling reconstruction design as we conclude in Section 5.5.

3.2.3 Function Space Generated by m_α

In this subsection, we explore the function space spanned by $\tilde{h}$ under the transformation $\tilde{m}_\alpha$. We observe that the matrix representation of $\tilde{m}_\alpha$ is a unitriangular matrix which belongs to the unitriangular matrix group. It indicates that if we operate on $f(t)$ with a sequence of $\tilde{m}_{\alpha_n}$, the scaled amplitude-function obtained after the transformation sequence can be achieved by a single transformation. That is,

$$
\begin{bmatrix} y \\ \tilde{h}(y) \end{bmatrix} = \begin{bmatrix} 1 & \frac{1}{\alpha_1} \\ 0 & 1 \end{bmatrix} \begin{bmatrix} 1 & \frac{1}{\alpha_2} \\ 0 & 1 \end{bmatrix} \cdots \begin{bmatrix} 1 & \frac{1}{\alpha_n} \\ 0 & 1 \end{bmatrix} \begin{bmatrix} t \\ f(t) \end{bmatrix} = \begin{bmatrix} 1 & \frac{1}{\alpha_1} + \frac{1}{\alpha_2} + \cdots + \frac{1}{\alpha_n} \\ 0 & 1 \end{bmatrix} \begin{bmatrix} t \\ f(t) \end{bmatrix}.
$$

In other words, composing $\tilde{m}_\alpha$ does not expand the function space of scaled amplitude-time functions. We also notice that time-amplitude functions are also in this space. Therefore, exploring properties of amplitude-time functions by first assuming α to be any sufficiently large number will not lose any generosity. Moreover, even when α is not accurate, we may still be able to modify the obtained amplitude-time function by composing it with some error-correcting $\tilde{m}_\beta$ transformation if β is carefully chosen.

3.3 Figurative Interpretation of m_α

As we discuss in this section the transformation $\tilde{m}_\alpha$ transformation can be interpreted in a figure. Given a value $y = t_0$, the value $\tilde{h}(t_0)$ can be obtained from the plot of $f(t)$.

From the relationship shown in Eq. (3.6), finding $\tilde{h}(t_0)$ is equivalent to finding t_1 so that $t_0 = t_1 + \frac{1}{\alpha} f(t_1)$ and then taking the value $f(t_1)$ as $\tilde{h}(t_0)$. As shown in Figure 3-2, t_1 can be determined by drawing a line with a slope $-1/\alpha$ through $(t_0, 0)$. With the knowledge of t_1, the value $\tilde{h}(t_0) = \tilde{h}(t_1 + \frac{1}{\alpha} f(t_1)) = f(t_1)$ can be observed as indicated in the plot. This interpretation is useful in designing an iterative algorithm for m_α implementation, which is shown in Section 3.4. This will be removed if I don't have time. Moreover, with the help of plots, it can lead to a discussion
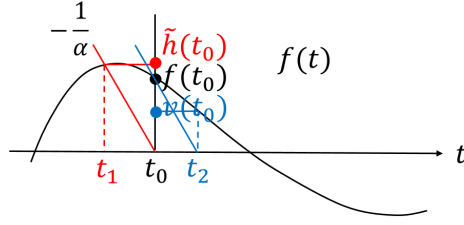
Figure 3-2: Determination of the value $\tilde{h}(t_0) = f(t_0 - \frac{1}{\alpha}f(t_0))$ and the value $v(t_0) = f(t_0 + \frac{1}{\alpha}f(t_0))$ from the plot of $f(t)$
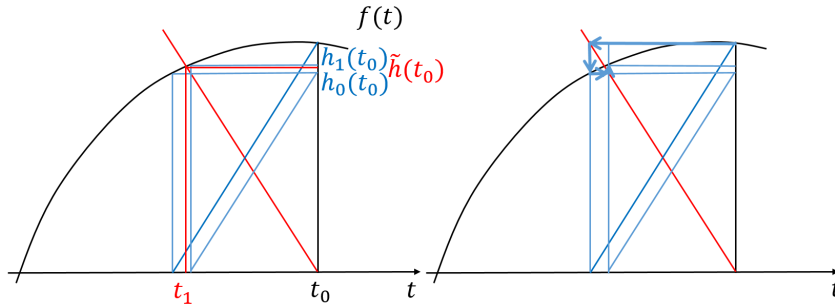
Figure 3-3: An illustration of how the value $h_n(t_0) = f(t_0 - \frac{1}{\alpha}h_{n-1}(t_0))$ approaches $\tilde{h}(t_0)$ through iterations.

about the change of difference between two functions before and after the transformation.

3.4 An Iterative Algorithm

In this section, we propose an iterative method to realize m_α since it may be difficult to directly implement the transformation, which is defined by taking the inverse function of the input function and subtracting the inverse function with a ramp. To be more precise, the algorithm shown in this section implements $\tilde{m}_\alpha$; to realize m_α, the function $\tilde{h}$ that is obtained from the implementation needs to be scaled back to h according to Eq. (3.5). Since $\tilde{m}_\alpha$ and $\tilde{m}_{-\alpha}$ differ only in sign, if $h(y)$ can be iteratively constructed from $f(t)$, $f(t)$ can be iteratively constructed from $h(y)$. Here we take advantage of the figurative interpretation of m_α to illustrate the method.

As discussed in Section 3.3 and shown in Figure 3-2, the value $\tilde{h}(t_0)$ can be obtained from the plot of $f(t)$. Since this figurative interpretation is obtained from Eq.

(3.6), which has a functional composition form, we first interpret functional composition in a plot. The value $v(t_0) = f(t_0 + \frac{1}{\alpha}f(t_0))$ can be observed by drawing a line with slope $-1/\alpha$ through $(t_0, f(t_0))$. Therefore $t_2 = t_0 + \frac{1}{\alpha}f(t_0)$ is determined and thus the value $v(t_0) = f(t_0 + \frac{1}{\alpha}f(t_0)) = f(t_2)$ is attained as shown in Figure 3-2. Figure 3-2 also shows that $\tilde{h}(t_0)$ is obtained by finding a value before the time t_0 while $v(t_0)$ is obtained by finding a value after the time t_0. Therefore, instead of finding $f(t_0 + \frac{1}{\alpha}f(t_0))$, we pursuit the value $h_0(t_0) = f(t_0 - \frac{1}{\alpha}f(t_0))$, which can be shown in Figure 3-3.

Now we iteratively update our approximation of $\tilde{h}$ by composing f with the function obtained from the last iteration. As shown in Figure 3-3, if f is composed with $t - \frac{1}{\alpha}h_0(t)$, the value $h_1(t_0) = f(t_0 - \frac{1}{\alpha}h_0(t_0))$ can still be observed in the plot of f. Moreover, the iteration $h_{n+1}(t_0) = f(t_0 - \frac{1}{\alpha}h_n(t_0))$ appears to converge to $\tilde{h}(t_0)$, where n denotes the index of the iteration. We now prove that not only such iteration uniquely converges to $\tilde{h}(t)$, its convergence rate can also be determined.

First, we recognize that as n goes to infinity the second equation of Eq. (3.6) and the iteration $h_{n+1}(t) = f(t - \frac{1}{\alpha}h_n(t))$ become the same if the limit exists. Moreover, Figure 3-3 suggests an explanation by the fixed-point theorem [30]. This can be achieved by reformulating the problem as finding t_1 such that $t_1 = t_0 - \frac{1}{\alpha}f(t_1) := p_{t_0}(t_1)$. If $p_{t_0}(t)$ satisfies the Lipschitz condition [31], i.e.

$$|p_{t_0}(a) - p_{t_0}(b)| \leq \lambda|a - b| \tag{3.14}$$

for some $|\lambda| < 1$, where $\lambda = \sup \frac{|f'(t)|}{\alpha}$, then the iteration will uniquely converge to the fixed point $p_{t_0}(t_1) = t_1$. Since $g(t)$ is required to be invertible, which implies $f'(t) + \alpha > 0$ for all t, we only need to add a constraint on the positive derivative of $f(t)$ to ensure $\alpha > \sup|f'(t)|$ so that $|\lambda| < 1$ can be satisfied. We also observe that the algorithm is of linear convergencce with a convergence rate λ. This once again indicates advantages of choosing larger α since λ decreases as α is increased.

As we mention in the beginning of this chapter, with this iterative algorithm to realize the transformation m_α, we will assume this transformation is implementable

when we discuss algorithms for the amplitude sampling reconstruction in Chapter 5.

Chapter 4

Frequency Domain Properties of Amplitude-time Functions

In this chapter, we discuss the frequency domain properties of amplitude-time functions. Since the goal is to design reconstruction algorithms to recover f from uniform samples of h, if h is bandlimited then f can be reconstructed by applying bandlimited interpolations of samples $h(n\Delta)$ and operating $m_{1/\alpha}$ to retrieve f. However, in this chapter we first prove that h is not bandlimited when f is bandlimited unless f is a constant. Nevertheless, the Fourier transform of h is shown to exponentially decay in frequency [11] with faster decay with increasing α. A sketch of the proof of the exponential decay rate is provided in Section 4.2. Simulation results are shown to verify the theoretical result in Section 4.3. These properties indicate that although an amplitude-time function generally cannot be reconstructed from its uniform amplitude samples by bandlimited interpolation if f is assumed to be bandlimited, the aliasing introduced from sampling can be negligible if the sampling rate is sufficiently high. A bandlimited-interpolation approximation of h based on samples $h(n\Delta)$ can achieve high signal-to-error ratio if Δ is sufficiently small. This observation leads to a reconstruction algorithm, the bandlimited-interpolation approximation (BIA) algorithm, that will be introduced and verified in Chapter 5 through simulations.

4.1   Bandwidth of $h(y)$

As noted earlier, $h(y)$ is not bandlimited unless $f(t)$ is a constant. We prove it in this section by contradiction. If $h(y)$ is assumed to be bandlimited, $h(y)$ would be an entire function of first order after analytically extending $h(y)$ to the entire complex plane [32]. Since f is assumed to be bandlimited, after analytic extension $f(t)$ and $f(t) + \alpha t$ are also entire functions of first order. Moreover, the composition of two entire functions remains an entire function. Therefore, $u(z) = h(f(z) + \alpha z)$ will be entire if h is entire. From Eq. (1.2), we know that $u(z)|_{z \in \mathbb{R}} = -\frac{1}{\alpha} f(z)$. Both $h(f(z) + \alpha z)$ and $-\frac{1}{\alpha} f(z)$ are entire; that is, they are analytic on the whole complex plane. Furthermore, the values on the real line of $h(f(z) + \alpha z)$ and $-\frac{1}{\alpha} f(z)$ are the same. By analytic continuation[1], it implies $h(f(z) + \alpha z) = -\frac{1}{\alpha} f(z)$ on the whole complex plane. However, from [34], if $h(f(z) + \alpha z)$ is an entire function of finite order and both h and f are entire functions, then either $f(z)$ is polynomial or $h(z)$ is of zero order. Since $f(z)$ is bandlimited, $f(z)$ being polynomial will imply it to be a constant function. Therefore, $h(z)$ is bandlimited if and only if $f(z)$ is a constant. In that case h is also a constant.

4.2   Decay Rate of Fourier Transform $\hat{h}(\xi)$

Although $h(y)$ is not bandlimited in general, it is shown in [11] that its Fourier transform exponentially decays as frequency increases. In this section, we present a sketch of the proof which somewhat different from in [11]. From [32], we have the following theorem:

Theorem 4.1. **[32]** *The Fourier transform of $h(y)$ exponentially decays, i.e. $\hat{h}(\xi) e^{\sigma |\xi|} \in L_2$, if and only if the following two conditions are satisfied:*

(a) $h(y)$ can be analytically extended in a strip $|\Im\{y\}| < \sigma$.

(b) $\|h(y)\|_\infty \leq C$ uniformly in the strip where C is a constant.

---

[1]The theorem of analytic continuation can be found in most complex analysis book, e.g. [33].
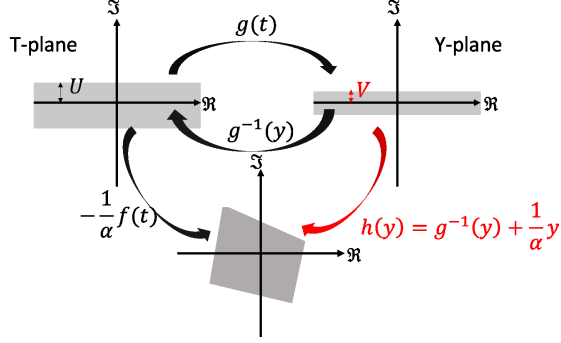
Figure 4-1: The amplitude-time function $h(y)$ is by definition $-\frac{1}{\alpha}f(g^{-1}(y))$. To show that the Fourier transform of $h(y)$ exponentially decays, we need to find a strip in Y-plane where $g^{-1}(y)$ can be analytically extended; the width of the strip is V.

Here $\hat{h}(\xi)$ is the Fourier transform of h with ξ being its radiant frequency. The variable y here is extended to the complex plane, i.e. $y = y_1 + iy_2$ where $y_1, y_2 \in \mathbb{R}$, and $\Im\{y\} = y_2$.

Here we only outline a procedure to show (a).

From Eq. (1.2), Figure 4-1 is obtained. Since $f(t)$ is assumed to be bandlimited to W, it is an entire function and is analytic on the entire complex plane. If we can find a strip with width $V > 0$ where g^{-1} is well-defined and analytic[2], then $h(y) = g^{-1}(y) + \frac{1}{\alpha}y$ is analytic in a strip with width $V > 0$, which satisfies (a). By (a) the width will then indicate the decay rate of the Fourier transform of h.

From the Inverse Function Theorem [33], if $g'(t) \neq 0$, $g(t)$ is locally injective. However, locally injective generally cannot imply globally injective; $g(t)$ is required to be globally injective on the preimage of the strip in Y-plane to ensure g^{-1} to be well-defined on the strip. Here we only show a method to determine a region in Y-plane where g^{-1} can be locally well-defined and thus h is locally well-defined. A proof to show $h(y)$ is well-defined in the strip, i.e. $g(t)$ is globally injective on the preimage of the strip in Y-plane, can be found in [11]. Since the boundary is mapped to the boundary by Open Mapping Theorem [33] and also by the fact that h is continuous, a lower bound of the width of the strip can be found in Y-plane.

---

[2]Y-plane denotes the complex plane extension of y and T-plane denotes the complex plane extension of t.

If $f(t)$ is bandlimited to W, by Bernstein's inequalities [13],

$$|f(t)| \le \|f\|_{C(\Re)} e^{W|\Im\{t\}|}. \tag{4.1}$$

$$|f'(t)| \le W\|f\|_{C(\Re)} e^{W|\Im\{t\}|}, \tag{4.2}$$

where $\|f\|_{C(\Re)}$ refers to the infinity norm when f is restricted to the real line. Then

$$g'(t) = f'(t) + \alpha. \tag{4.3}$$

$$|g'(t)| \le |f'(t) + \alpha| \le |f'(t)| + \alpha \le W\|f\|_{C(\Re)} e^{W|\Im\{t\}|} + \alpha \tag{4.4}$$

$$= AW e^{W|\Im\{t\}|} + \alpha, \tag{4.5}$$

where we let $A = \|f\|_{C(\Re)}$.

By Eq. (4.2) we know if

$$|\Im\{t\}| \le \frac{1}{W} \log \frac{\alpha}{AW}, \tag{4.6}$$

then

$$f'(t) \le AW e^{W|\Im\{t\}|} \tag{4.7}$$

$$\le \alpha. \tag{4.8}$$

Then $g'(t) \ne 0$. Therefore, $g(t)$ is locally injective in a strip with width $|U| = \frac{1}{W} \log \frac{\alpha}{AW}$. To determine V, we need to find $V = \min_{|\Im\{t\}|=U} |\Im\{g(t)\}|$. By (4.1),

$$|\Im\{g(t)\}| \ge -|\Im\{\|f\|_{C(\Re)} e^{W|\Im\{t\}|}\}| + |\Im\{\alpha t\}|$$

$$\ge -A e^{W|U|} + \alpha|U|$$

$$= \frac{\alpha}{W} \log \frac{\alpha}{AW} - \frac{\alpha}{W}$$

$$= V, \tag{4.9}$$

where $\Im\{t\} = U$.

The decay rate shown in Eq. (4.9) is slightly smaller than the result shown in [11]. This is because only the zeroth and the first order of Bernstein's inequalities are utilized. [11] uses more orders of Bernstein's inequalities to show global invertibility and determines the decay rate. However, after h is scaled as in Eq. (3.5), the decay rate shown in Eq. (4.9) and the decay rate shown in [11] will be the same as α goes to infinity.

4.3 Simulations

In this section, simulation results are shown to verify the bound given by [11]. Amplitude-time functions obtained from the same $f(t)$ with different choices of α are compared. We also compare amplitude-time functions obtained from the same m_α transform but with their corresponding time-amplitude functions having different frequency components.

From [11], if f is bandlimited to W and $|f| \leq A$, then

$$|\hat{h}(\xi)| = O(e^{-|\xi|(\frac{\alpha}{W}\log(\frac{\alpha}{AW})-\frac{\alpha-AW}{W})}), \tag{4.10}$$

where $\hat{h}(\xi)$ stands for the Fourier transform of $h(y)$ and ξ is the angular frequency. To match with Theorem 4.1, we will denote $\sigma = \frac{\alpha}{W}\log(\frac{\alpha}{AW}) - \frac{\alpha-AW}{W}$ as the decay rate factor. By the definition of the big-O notation, Eq. (4.10) is equivalent to the following statement: $\exists \xi_0$ such that $\forall \xi > \xi_0$,

$$|\hat{h}(\xi)| < C(e^{-|\xi|(\frac{\alpha}{W}\log(\frac{\alpha}{AW})-\frac{\alpha-AW}{W})}), \tag{4.11}$$

for some constant C. The coefficients C and ξ_0 can be chosen so that $|\hat{h}(\xi_0)| = C(e^{-|\xi_0|(\frac{\alpha}{W}\log(\frac{\alpha}{AW})-\frac{\alpha-AW}{W})})$.

Compared with Eq. (4.9), the above differs from Eq. (4.9) by a value A, which can not be neglected if α is not larger than AW. It can be neglected as α goes to infinity. An important fact is that although we consider the factor AW in Eq. (4.10), this factor is in the equation because Eq. (4.10) is derived from Bernstein's

inequality of the first derivative of f as shown in Section 4.2. Therefore, when we cannot estimate the maximum negative first derivative, we can use the Bernstein bound AW. When we have a better bound of the first derivative, we should instead use that bound to approach a larger exponential decay rate. It also indicates that when $f(t) = A\sin(Wt)$, the exponential decay rate shown in Eq. (4.10) is tight. We give another observation as followed:

$$
\begin{aligned}
\sigma &= \frac{\alpha}{W} \log \frac{\alpha}{AW} - \frac{\alpha - AW}{W} \\
&\leq \frac{\alpha}{W}(\frac{\alpha}{AW} - 1) - \frac{\alpha - AW}{W} \\
&= \frac{\alpha}{W}(\frac{\alpha - AW}{AW}) - \frac{\alpha - AW}{W} \\
&= A(\frac{\alpha}{AW} - 1)^2.
\end{aligned}
\tag{4.12}
$$

The inequality comes from the Taylor series expansion of $\log x$ around $x = 1$ and is true for all $x > 0$. We first notice from Eq. (4.12) that the bound σ will never be negative since we require $\alpha > AW$ for amplitude sampling to be well-defined. Moreover, when $\frac{\alpha}{AW}$ goes to 1, $\sigma \simeq A(\frac{\alpha}{AW} - 1)^2$ since the zeroth and first order of the Taylor series can well approximate $\log x$ around 1 and thus the Fourier transform will decay slowly. This effect can be observed when we analyze our reconstruction algorithms in Section 5.4.

According to Eq. (4.10), as α increases, the magnitude of $\hat{h}(\xi)$ decays faster. We first compare $g_a(t) = \sin(2\pi t) + 8t$ with $g_b(t) = \sin(2\pi t) + 32t$. However, as shown in Section 3.1, the corresponding period of h_b is 32 while that of h_a is 8. In order to compare these functions based on the same frequency scale, we instead compare $\tilde{h}(y)$ as defined in Eq. (3.5). The following decay rates are then acquired from Eq. (4.10):

$$
\begin{cases}
|\hat{\tilde{h}}_a(\xi)| = O(e^{-|\xi|(\frac{8}{2\pi} \log(\frac{8}{2\pi}) - \frac{8}{2\pi} + 1)}). \\
|\hat{\tilde{h}}_b(\xi)| = O(e^{-|\xi|(\frac{8}{2\pi} \log(\frac{32}{2\pi}) - \frac{8}{2\pi} + \frac{1}{4})}).
\end{cases}
\tag{4.13}
$$

As shown in Figure 4-2, $|\hat{\tilde{h}}_b(\xi)|$ decays faster than $|\hat{\tilde{h}}_a(\xi)|$. Both of them satisfy Eq. (4.13).
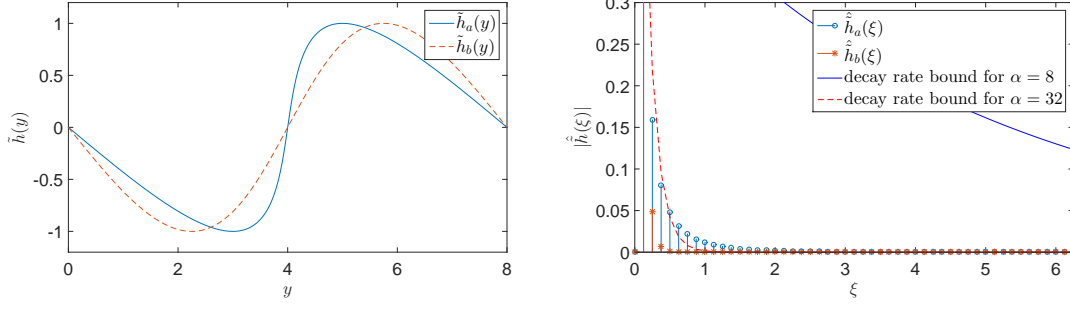
Figure 4-2: Comparison between two amplitude-time functions transformed from $f(t) = \sin(2\pi t)$ with m_8 and m_{32} respectively
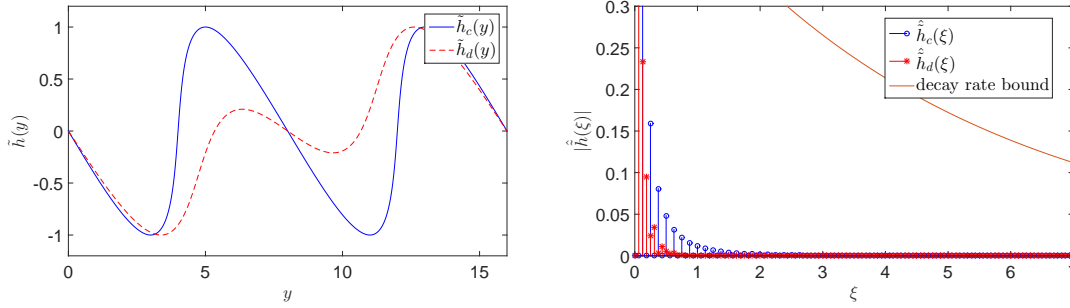
Figure 4-3: Comparison between amplitude-time functions transformed from $f(t)$ with different frequency components with the same transformation m_{16}

We then compare how frequency components of f affect the decay rate. In order to compare $\sin(4\pi t)$ with $\sin(2\pi t) + \sin(4\pi t)$, the latter is scaled so that the maximum amplitude is not greater than 1. Then we obtain $g_c(t) = \sin(4\pi t) + 16t$ and $g_d(t) = C(\sin(4\pi t) + \sin(2\pi t)) + 16t$. Here C is the scaling factor that makes $\|g_d(t)\|_{C(\Re)} = 1$. From (3.13), the decay rate is larger as the frequency scaling factor B is larger and the amplitude scaling factor A is smaller. That is, the decay rate is larger as the low frequency components is larger. Therefore, when $AW = D$ is fixed and when the bandwidth is required to be smaller than $\tilde{W}$, the decay rate of the Fourier transform of $\tilde{h}(y)$ intuitively should be the smallest when it is transformed from $f(t) = \frac{D}{\tilde{W}} \sin(2\pi \tilde{W} t)$. As shown in Figure 4-3, $|\hat{\tilde{h}}_c(\xi)|$ decays faster than $|\hat{\tilde{h}}_d(\xi)|$ does, which satisfies the statement above. This observation suggests a conjecture in Section 5.4.1.1 and will be helpful for simulation analysis.

Chapter 5

Amplitude Sampling Reconstruction Algorithms

As mentioned in Section 1.1, to reconstruct the original signal from uniform samples of its amplitude-time function, two steps are involved. The first step is to implement m_α. In Section 3.4 we have already provided an iterative algorithm to implement m_α. In this chapter, we assume that m_α is implementable and we focus on the second step, reconstructing a continuous signal from a discrete representation, which is our main goal: amplitude sampling reconstruction. Two reconstruction algorithms are introduced. The first algorithm, the Bandlimited-Interpolation Approximation (BIA), approximates $h(y)$ by the bandlimited interpolation of $h(n\Delta)$ and transforms the resulting approximate amplitude-time function $\check{h}(y)$ into the approximate signal $\check{f}(t)$ by the transformation $m_{1/\alpha}$. Another reconstruction algorithm, the Iterative Amplitude Sampling Reconstruction (IASR), attempts to iteratively remove out-of-band components by low-pass filtering (with cutoff frequency W) the approximate time-amplitude function $\check{f}(t)$ obtained from the BIA and updating the approximated function by comparing the samples of its amplitude-time representation with the original samples $h(n\Delta)$. Since our sampling space is different from the bandlimited signal space (m_α is not linear), it is difficult to find a direct exact reconstruction algorithm. However, we can utilize our understanding on m_α as discussed in Chapters 3 and 4 to analyze our iterative reconstruction algorithm.

Nevertheless, there is another way to reconstruct f. As discussed in Section 1.1, each sample $(n\Delta, h(n\Delta))$ can be bijectively mapped to a nonuniform sample point $(t_n, f(t_n))$ in f. Therefore, other than reconstructing f directly from the uniform samples of h, an alternative is to first transform the uniform samples of h into the nonuniform samples of f and then implement nonuniform time sampling reconstruction methods. Since our proposed algorithm is iterative, it is reasonable to compare our performance with an iterative nonuniform time sampling reconstruction algorithm. Moreover, since the adaptive weights method (AWM) was shown to perform the best in numerical results [12], we compare our algorithms with the AWM. Both the algorithm and the proof of the convergence of the AWM can be found in Section 2.2. Simulation settings are provided in Section 5.3 and simulation results of our proposed methods and the AWM are shown in Section 5.4.

5.1 the Bandlimited-Interpolation Approximation (BIA) Algorithm

In this section we introduce the bandlimited-interpolation approximation (BIA) algorithm that can approximate f arbitrarily well without iterations if the sampling rate is sufficiently large. Since f can be obtained from h by $m_{1/\alpha}$, one approach to recovering f is to first approximate h from its samples. One approximation of $h(y)$ is the bandlimited-interpolation of its uniform samples $\{h(n\Delta)\}$. However, since the bandlimited-interpolation function $\check{h}(y)$ is by definition bandlimited, it cannot be the same as $h(y)$ since $h(y)$ is not bandlimited unless f is a constant as explained in Section 4.1. Nevertheless, according to [11], $\|\check{h}(y) - h(y)\|_\infty \le Ce^{-\frac{\sigma}{\Delta}}$ for some constant $C > 0$ where $\sigma = \frac{\alpha}{W}\log(\frac{\alpha}{AW}) - \frac{\alpha - AW}{W}$. That is, the error measured in the L_∞ norm between $\check{h}(y)$ and $h(y)$ decreases exponentially fast as $1/\Delta$ increases. The signal $f(t)$ then is approximated by $\check{f}(t)$, the function transformed from $\check{h}(y)$ by $m_{1/\alpha}$. Similarly, $\check{f}(t)$ cannot be the same as $f(t)$ since $\check{f}(t)$ will not be bandlimited.

It should be noticed that $\check{h}(y) + y/\alpha$ should be invertible. This would affect the
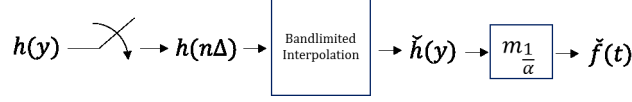
Figure 5-1: Bandlimited-interpolation approximation (BIA) algorithm flow diagram
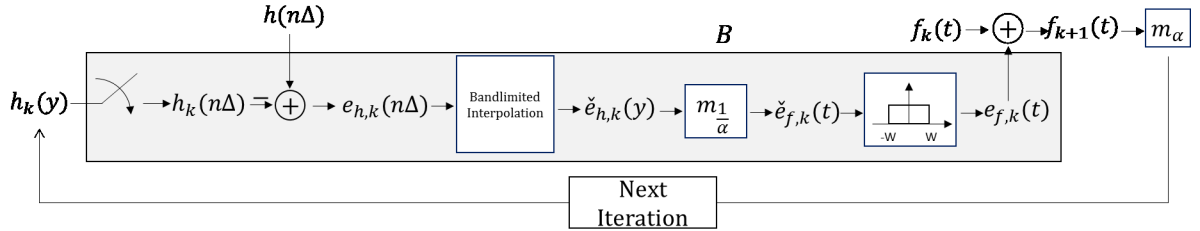
Figure 5-2: Iterative Amplitude Sampling Reconstruction Algorithm (IASR) flow diagram

range of Δ we can choose when we implement amplitude sampling. A necessary and sufficient condition on Δ has not yet been found to ensure the invertibility. Moreover, the error bound between $f(t)$ and $\check{f}(t)$ is still unknown. However, our simulation result shows that the error can be arbitrarily small if samples are sufficiently dense; this result is consistent with the intuition that the energy outside an adequately high band is negligible due to the exponential decay rate of the Fourier transform of amplitude-time functions as discussed in Section 4.2. Simulation results are shown in Section 5.4.

5.2 the Iterative Amplitude Sampling Reconstruction (IASR) Algorithm

From Section 5.1, the BIA cannot be exact because the resulting function $\check{f}(t)$ is not bandlimited. To improve the reconstruction, a new approximation $\check{f}_0(t)$ is obtained from $\check{f}(t)$ by processing $\check{f}(t)$ through a low-pass filter. Since the values of the samples $h(n\Delta)$ are known, it suggests transforming $\check{f}_0(t)$ back to the amplitude domain by m_α and re-sampling to obtain $\{\check{h}_0(n\Delta)\}$. Since $\{\check{h}_0(n\Delta)\}$ are not the same as $\{h(n\Delta)\}$, this suggests an iterative algorithm in which $\check{h}_0(n\Delta)$ is subtracted from $h(n\Delta)$ and interpolating the error samples $e_{h,1}(n\Delta) = \check{h}_0(n\Delta) - h(n\Delta)$, repeating the process to

obtain $e_{f,1}(t)$ and then adding it back to $\breve{f}_0(t)$. The iteration process is summarized in Figure 5-2.

A necessary condition determining whether this iterative algorithm reconstructs $f(t)$ follows from Theorem 2.2 and Theorem 2.5. If there exists $h_2(y)$ transformed from a bandlimited function $f_2(t) \neq f(t)$ such that $h_2(n\Delta) = h(n\Delta)$ for each n, we cannot determine whether the reconstructed function is f or f_2. Since the sampled sequence $\{(n\Delta, h(n\Delta))\}$ can be bijectively mapped to a sequence $\{(t_n, f(t_n))\}$, conditions for the IASR to be able to reconstruct the original signal then become conditions for these nonuniform timings $\{t_n\}$ to be a uniqueness sequence and also a sampling sequence, since as discussed in Section 2.1 stable reconstruction is crucial in practice. Because a sampling sequence implies a uniqueness sequence, we can find the conditions for $\{t_n\}$ based on Theorem 2.5 by measuring the Beurling lower density as follows.

Since $f(t_n) + \alpha t_n = n\Delta$, we then have $t_n = \frac{n\Delta - f(t_n)}{\alpha}$. To find the number of sampling between time a and time $a + r$ is equivalent to find the number of integer n such that

$$a \leq \frac{n\Delta - f(t_n)}{\alpha} \leq a + r.$$
$$\Rightarrow \frac{-A + \alpha a}{\Delta} \leq \frac{f(t_n + \alpha a)}{\Delta} \leq n \leq \frac{\alpha(a + r) + f(t_n)}{\Delta} \leq \frac{\alpha(a + r) + A}{\Delta}, \qquad (5.1)$$

where the leftmost and rightmost inequality follows from $\|f\| \leq A$. From Eq. 5.1, we obtain

$$\frac{1}{r}\lceil \frac{2A + \alpha r}{\Delta} \rceil \leq \frac{1}{r}\sharp\{\{t_n\} \cap [a, a + r]\} \leq \frac{1}{r}(\lceil \frac{2A + \alpha r}{\Delta} \rceil + 1) \qquad (5.2)$$

for every a and r. From Eq. 5.2 we then obtain

$$D_-(\{t_n\}) = \liminf_{r \to \infty} \inf_a \frac{1}{r}\sharp\{\{t_n\} \cap [a, a + r]\} = \frac{\alpha}{\Delta}. \qquad (5.3)$$

Therefore, if $\frac{\alpha}{\Delta} > \frac{W}{\pi}$ and if the iterative reconstruction algorithm converges, the function that the reconstruction algorithm converges to will be $f(t)$.

However, to analyze the convergence of the algorithm, we cannot emulate the conventional analysis on iterative nonuniform sampling algorithms as outlined in

48

Proposition 2.6. As shown in Figure 5-2, our iteration can be formulated as $f_{k+1} = f_k + B(h - m_\alpha f_k) = f_k + B(m_\alpha f - m_\alpha f_k)$. It is different from $f_{k+1} = f_k + A(f - f_k)$ as in Eq. (2.4). A way to prove the convergence of the IASR is to show $\|B(m_\alpha f - m_\alpha f_k)\| \leq \|B\| \|m_\alpha f - m_\alpha f_k\| < \gamma \|f - f_k\|$ for some $\gamma < 1$. Note that since B consists of bandlimited interpolation, low-pass filtering, and an $m_{1/\alpha}$ transformation, it is easier to analyze L_2 norm of B. However, although we can show that the L_1 norm of $\|m_\alpha f - m_\alpha f_k\|$ is the same as the L_1 norm of $\|f - f_k\|$, the nonlinearity of m_α makes it difficult to analyze $\|m_\alpha f - m_\alpha f_k\|$ in L_2 norm and therefore the convergence of the IASR has not yet been proven. However, simulation results shown in Section 5.4 indicate that our IASR algorithm converges and outperforms the AWM in the convergence rate if α is properly chosen.

5.3 Simulation and Comparison of the BIA, IASR, and AWM Algorithms

As discussed in the beginning of this chapter, we evaluate the two proposed algorithms through simulations and compare them with a nonuniform sampling reconstruction method, the AWM, based on different parameter settings. In this section we first describe the generation of the tested signals $f(t)$ and the samples $\{h(n\Delta)\}$. Our goal is to reconstruct the signal $f(t)$ from its corresponding samples $\{h(n\Delta)\}$. How these algorithms are numerically implemented is then discussed. The flow diagrams for the BIA algorithm, the IASR algorithm, and the AWM are shown in Figure 5-1, Figure 5-2, and Figure 2-1 respectively. Moreover, since the AWM requires the largest time difference δ between two consecutive nonuniform samples to be smaller than π/W and our controlled parameter is Δ, conditions on Δ to achieve this constraint will be provided in this section.

5.3.1 Input Signal Generations

As discussed in Section 1.1, we study the performance of our reconstruction algorithms on the recovery of bandlimited signals. Both randomly generated bandlimited signals and deterministic sinusoidal signals are tested. The former can evaluate general parameter effects while the latter can assess the worst case. This objective will be made clear in Section 5.4.

To simulate a randomly generated bandlimited signal $f(t)$, a sequence of 10000 points $\{f(\hat{t}_n)\}$ with amplitude values lying between -0.5 and 0.5 is uniformly generated, where $\hat{t}_n = 0.0001n$ are the sufficiently fine timings such that $\{f(\hat{t}_n)\}$ well approximates the continuous signal $f(t)$ [1]. The simulated timing ranges from 0 to 0.9999 and $f(t)$ is assumed to be periodic with a period 1. Therefore, $\{f(\hat{t}_n)\}$ approximate one period of $f(t)$ [2]. In order to obtain a bandlimited signal, the sequence is then filtered by a low-pass filter with a specified bandwidth W, which will later be one of our controlled parameters. Then the amplitude of the sequence is scaled so that the maximum value of $|f'(t)|$ is 0.5. Therefore as long as the parameter α in the transformation m_α is chosen to be greater than 0.5 the corresponding function h is well-defined.

In addition to randomly generated signals, we have tested reconstruction algorithms on deterministic sinusoidal signals so that the effect of each parameter can be more carefully evaluated. In the case of deterministic input signals, we fix most of our reference signals as $f(t) = \sin(2\pi t)/8$, and study how the reconstruction performance of all three methods changes when we vary the controlled parameters. These discussions will be provided in Section 5.4.2.

---

[1]The notation $\hat{t}_n$ is used to distinguish from the nonuniform timing t_n.

[2]If a function is not periodic but is bandlimited, it will not be time-limited. (The definition of time-limited signal can be found in a footnote in Chapter 2.) In that case, we cannot simulate it without numerical errors since we will need to truncate its time-domain representation and will need to take samples on its frequency-domain representation. Because in both time and frequency domain we can only simulate a finite-length sequence of discrete samples, the assumption of a function being periodic will be without loss of generality.
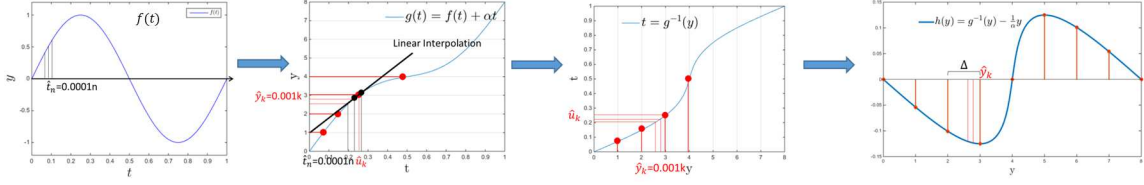
Figure 5-3: m_α and $h(n\Delta)$ simulations

5.3.2 Simulations of m_α and $h(n\Delta)$

With f simulated, we also need to simulate its corresponding amplitude-time function samples $h(n\Delta)$ so that the performance of the three algorithms can be tested. As shown in (a) of the Figure 5-2, after f is simulated, the transformation m_α from $f(t)$ to $h(y)$ should be realized. This is achieved by approximating $h(y) = g^{-1}(y) - \frac{1}{\alpha}y$ with sufficiently close sample points $\{h(0.001k)\}$ where k ranges from 1 to 1000α; α is chosen to be an integer in our simulations. Since the period T_1 of f is assumed to be 1, h will be periodic with a period $T_2 = \alpha * T_1 = \alpha$; thus $\{h(0.001k)\}$ approximate one period of h. To obtain these values $\{h(0.001k)\}$, a ramp αt is first added to the simulated input signal $f(t)$ to acquire $g(t) = f(t) + \alpha t$. As discussed in Section 5.3.1, its discrete approximation in our simulation will then be $\{g(0.0001n)\}$ as indicated in Figure 5-3. A sequence $\{u_k\}$ that satisfies $g(u_k) = 0.001k = \hat{y}_k$ is approximated by linear interpolation of $g(0.0001n)$ so that for each k between 1 and 1000α the value $g^{-1}(0.001k)$ can be approximated by u_k. The amplitude-time function $h(y)$ then can be approximated by $h(\hat{y}_k) = u_k - \frac{1}{\alpha}(\hat{y}_k)$.

To obtain the simulated samples $\{h(n\Delta)\}$ that will be used to test our algorithms, Δ will be chosen to be larger than 0.001 but small enough to ensure that $\{h(n\Delta)\}$ can be uniquely mapped to a bandlimited signal with a bandwidth smaller than or equal to W. The referenced Δ is 0.05; $\{h(n\Delta)\}$ are obtained by choosing one sample from every 50 fine instances $h(\hat{y}_k)$. The transformation $m_{\frac{1}{\alpha}}$ in Figure 5-1 and 5-2 is simulated in the same way as m_α except that the parameter α is replaced by $\frac{1}{\alpha}$.

5.3.3 the Bandlimited Interpolation Simulation for a Periodic Function

In the previous two subsection, the constructions of both $f(t)$ and samples $\{h(n\Delta)\}$ are described and the simulated f and $h(n\Delta)$ will later be regarded as the ground truth data. That is, $\{h(n\Delta)\}$ are used to reconstruct $f(t)$ and the error is considered as the difference between the reconstructed signal and $f(t)$. In this subsection, we focus on the numerical realization of our algorithms as in Figure 5-1 and Figure 5-2. To be more precise, we focus on the implementation of the bandlimited interpolation, which is defined as follows:

Given a sequence $x[n]$, its bandlimited interpolation $\hat{x}(t)$ is defined as

$$\hat{x}(t) = \sum_{n=-\infty}^{\infty} x[n] \frac{\sin(\pi(\frac{t}{\Delta} - n))}{\pi(\frac{t}{\Delta} - n)} = \sum_{n=-\infty}^{\infty} x[n] sinc(\frac{t}{\Delta} - n), \tag{5.4}$$

where $sinc(x) = \frac{\sin(\pi x)}{\pi x}$. We denote $x[n] = h(n\Delta)$ in Figure 5-4, and therefore $x(t)$ can be thought of as $h(y)$, which is not assumed to be bandlimited.

Instead of approximating $\hat{x}(t)$ by a finite summation of truncated sinc functions (since we cannot simulate an infinitely-long function) based on $x[n]$, we instead obtain $\hat{x}(t)$ by using the DFT. We show in this subsection the validity of this method. In fact, by doing so, the numerical error of simulating bandlimited interpolation for a periodic function will be from the implementation of DFT rather than the error of truncating a summation with infinite terms and a truncated interpolation function.

From Eq. (5.4), we know that obtaining the bandlimited interpolation $\hat{x}(t)$ of $x[n]$ is equivalent to taking the discrete time Fourier transform (DTFT) of $x[n]$, normalizing the frequency scale, and using a low-pass filter with scaling factor Δ and bandwidth $\frac{\pi}{\Delta}$, as shown in Figure 5-4 by the red arrows. We can therefore express

(A) and (C) in Figure 5-4 as:

$$(A) \quad x[n] \; = \; \frac{1}{2\pi} \int_0^{2\pi} \hat{X}(e^{j\omega}) e^{j\omega n} d\omega. \tag{5.5}$$

$$= \; \frac{1}{2\pi} \int_0^{2\pi} \sum_{k=0}^{M-1} b_k \delta(\omega - \frac{2\pi\Delta}{T}k) e^{j\omega n} d\omega. \tag{5.6}$$

$$= \; \frac{1}{2\pi} \sum_{k=0}^{M-1} b_k e^{j\frac{2\pi\Delta}{T}kn}. \tag{5.7}$$

$$(B) \quad x[n] \; = \; \frac{1}{M} \sum_{k=0}^{M-1} c_k e^{j\frac{2\pi}{M}kn}. \tag{5.8}$$

$$(C) \quad x(t) \; = \; \frac{\Delta}{2\pi} \int_0^{\frac{2\pi}{\Delta}} X(j\Omega) e^{j\Omega t} d\Omega. \tag{5.9}$$

$$= \; \frac{\Delta}{2\pi} \int_0^{\frac{2\pi}{\Delta}} \hat{X}(e^{j\Omega\Delta}) e^{j\Omega t} d\Omega. \tag{5.10}$$

$$= \; \frac{1}{2\pi} \int_0^{2\pi} \hat{X}(e^{j\omega}) e^{j\frac{\omega}{\Delta}t} d\omega. \tag{5.11}$$

$$= \; \frac{1}{2\pi} \sum_{k=0}^{M-1} b_k e^{j\frac{2\pi\Delta}{T}k\frac{t}{\Delta}}. \tag{5.12}$$

$$= \; \frac{1}{2\pi} \sum_{k=0}^{M-1} b_k e^{j\frac{2\pi k}{T}t}. \tag{5.13}$$

Note that here we utilize the fact that $x[n]$ is periodic with a period T and therefore its DTFT $\hat{X}(e^{j\omega})$ can be expressed as $\sum_{k=0}^{M-1} b_k \delta(\omega - \frac{2\pi\Delta}{T}k)$. We compare the expression of $x[n]$ in Eq. (5.7) with the discrete Fourier series (DFT) based on one period of $x[n]$ as shown in Eq. (5.8). We then obtain $\frac{b_k}{2\pi} = \frac{c_k}{M}$ where M is the number of samples in a period which is equal to $\frac{T}{\Delta}$. By replacing $\frac{b_k}{2\pi}$ in Eq. (5.13) with $\frac{c_k}{M}$, we then obtain

$$\hat{x}(t) = \sum_{k=0}^{M-1} \frac{c_k}{M} \exp^{j\frac{2\pi}{T}kt}. \tag{5.14}$$

Therefore, in order to obtain $\check{h}(y)$ from $\{h(n\Delta)\}$, we calculate the DFT of $h(n\Delta)$ with length $M = 1000\alpha$ as discussed in Section 5.3.2. Then we oversample $\check{h}(y)$ by a factor of 100 as shown in Figure 5-5 and use these samples to approximate the continuous function $\check{h}(y)$. Since we lose a factor of 10 sample points when linear

53
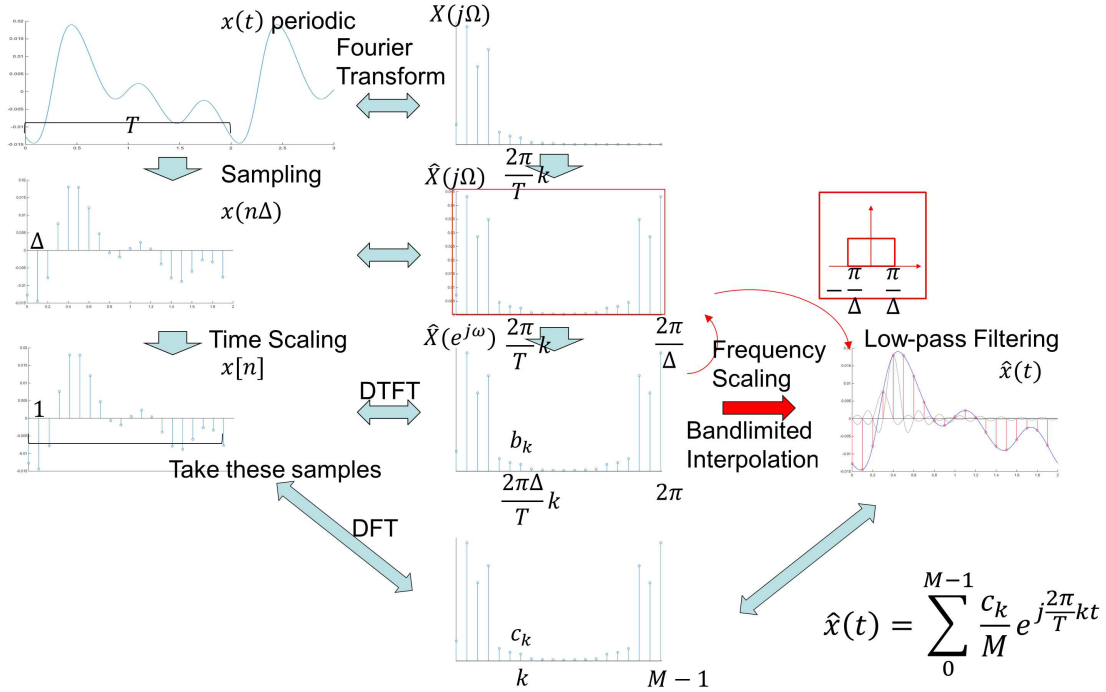
Figure 5-4: Bandlimited-interpolation implementation for periodic functions

interpolation is used to approximate the inverse functions both in m_α and $m_{1/\alpha}$, this oversampling cancels out this data loss and thus our $\check{f}(t)$ has the same sufficiently fine sampling rate as $f(t)$. The simulations of the low-pass filter and sampling are straight forward and are not discussed in this thesis.

5.3.4 Parameter Constraints on the AWM in Amplitude Sampling

As discussed in the beginning of this chapter, in order to better understand the performance of our proposed algorithms, we compare them with the adaptive weights method (AWM), which was proven by [12] to perform the best among iterative nonuniform sampling reconstruction algorithms. For the AWM to be applied as described in Theorem 2.7, the parameter δ should be sufficiently small. Since the nonuniform sampling $\{f(t_n)\}$ are mapped from uniform sampling $\{h(n\Delta)\}$, the time difference $\delta = \sup\{t_{n+1} - t_n\}$ of consecutive nonuniform samples on f can be estimated from Δ. In this subsection we discuss the relationship and provide a criterion that guarantees
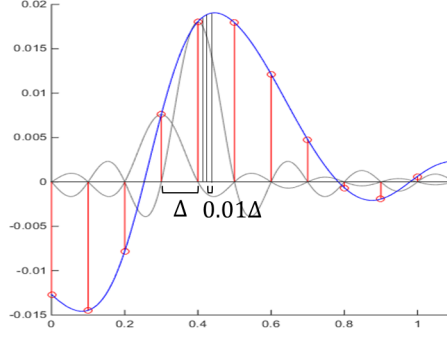
Figure 5-5: Simulation for bandlimited interpolation on $h(n\Delta)$

the applicability of Theorem 2.7.

The sufficient bound of Δ for Theorem 2.7 to be applicable can be derived as follows:

$$f(t_n) + \alpha t_n = n\Delta.$$

$$f(t_{n+1}) + \alpha t_{n+1} = (n+1)\Delta.$$

$$\Rightarrow t_{n+1} - t_n = \frac{\Delta - (f(t_{n+1}) - f(t_n))}{\alpha}. \tag{5.15}$$

By mean value theorem [35], there exists $\eta_n \in (t_n, t_{n+1})$ such that $f(t_{n+1}) - f(t_n) = f'(\eta_n)(t_{n+1} - t_n)$. Therefore, Eq. 5.15 can be rewritten as

$$t_{n+1} - t_n + \frac{f'(\eta_n)(t_{n+1} - t_n)}{\alpha} = \frac{\Delta}{\alpha}.$$

$$\Rightarrow t_{n+1} - t_n = \frac{\Delta}{\alpha} \frac{1}{1 + \frac{f'(\eta_n)}{\alpha}}. \tag{5.16}$$

The condition for Theorem 2.7 to be applicable then can be related to Δ as follows:

$$t_{n+1} - t_n = \frac{\Delta}{\alpha} \frac{1}{1 + \frac{f'(\eta_n)}{\alpha}} < \frac{\pi}{W}. \tag{5.17}$$

Also, since the condition $\left|\frac{f'(t)}{\alpha}\right| < 1 \forall t$ is required for amplitude sampling to be well-defined,

$$\frac{1}{1 + \frac{f'(\eta_n)}{\alpha}} > \frac{1}{2}. \tag{5.18}$$

From Eq. (5.17) and Eq. (5.18),

$$\frac{\Delta}{\alpha}\frac{1}{2} < \frac{\Delta}{\alpha}\frac{1}{1+\frac{f'(\eta_n)}{\alpha}} < \frac{\pi}{W}.$$

$$\Rightarrow \frac{\Delta}{\alpha} < \frac{2\pi}{W}. \tag{5.19}$$

Recall that from Theorem 2.5, a nonuniform time sequence is a sampling sequence if the Beurling lower density is larger than twice the bandwidth. As shown in Eq. (5.3), the Beurling lower density on the original function is $\frac{\alpha}{\Delta}$. A sufficient condition to apply Theorem 2.7 to show the uniqueness and stability of the nonuniform time sequence will then be $\frac{\Delta}{\alpha} < \frac{\pi}{W}$. However, for the AWM to be applicable, Eq. (5.19) is needed, which requires twice the sampling rate for samples to be a unique representation of a bandlimited function with a bandwidth W. It is because instead of using the average sampling rate Δ/α to prove the AWM, [12] used the maximum sampling time difference δ to pursue an explicit bound for the convergence rate. From Eq. (5.17), in amplitude sampling, the value of δ depends on how α is chosen and the value of the largest negative first derivative of f. This observation will be verified in our simulation results in Section 5.4.

5.4   Numerical Results on Reconstruction Algorithms

In this section simulation results based on different parameters α, Δ, W are shown. As discussed in Section 5.3.1, both randomly generated bandlimited signals and deterministic sinusoidal signals are tested. For both types of tested signals, we will evaluate single parameter effects on our algorithms (the IASR and the BIA) and on the nonuniform sampling method (the AWM in particular) by changing one of the three parameters at a time and comparing the signal-to-error ratio (SER) per iteration. Since the BIA implements the first iteration of the IASR without low-pass filtering $\check{f}$, it does not involve any iteration. Its reconstructed signal does not change over iterations and neither does its SER. Although the BIA does not improve over iterations, it is important to analyze its performance. Since the performance of the

BIA shows approximately the accuracy of the first approximation of the IASR, it can be used to evaluate parameter settings in which the reconstructed signal from the IASR is sufficiently close to the original signal after the first iteration and may already be satisfactory in some applications. Moreover, because the reconstructed function $\check{f}(t)$ is transformed from the amplitude-time function $\check{h}(y)$, which is the bandlimited approximation of $h(y)$, it indicates how close $h(y)$ is to a bandlimited function. Furthermore, by evaluating the number of iterations for the AWM to reach the same SER as the BIA, we can analyze how much our algorithms outperform the AWM based on amplitude sampling since the design of the AWM is under a general nonuniform sampling setting.

In Section 5.4.1, we will first show simulation results when input signals are randomly generated. In such case we also evaluate the robustness of our algorithms. However, to further analyze the parameter effects on our algorithms, for example parameter effects under some worst case scenarios, we specify the input signals and evaluate the reconstructions under more parameter settings such as changing the amplitude or fixing the value of the largest first derivative of f. Reasons for those settings along with simulation results based on those settings will be made clear in Section 5.4.2. We will summarize these discussions in Section 5.5 and present desirable parameter settings for amplitude sampling.

5.4.1 Randomly Generated Signals

We first present the simulation results when the bandlimited input signal is randomly generated as described in Section 5.3.1. Our default parameter setting is as follows: $\alpha = 4$, $\Delta = 1/20$, and $W = 16\pi$. In this subsection, we will discuss the simulation results when α, δ, W are individually changed and when α/Δ is fixed but α is changed. We will also evaluate the robustness of each algorithm by calculating the variance of the SER per iteration with the default parameter setting. We will discuss the effect of α on three algorithms in details. The analysis on effects of other parameters will be a modification of the effect of α.

5.4.1.1   Change of α

In this section, we discuss simulation results when α is changed from 4 to 2. We focus on two comparisons: the comparison between the BIA and the AWM, and the comparison between the convergence rate of the IASR and that of the AWM. As mentioned in the beginning of Section 5.4, the performance of the BIA in general is similar to that of the IASR after the first iteration. That is, we do not need to compare the performance of the IASR after one iteration with the AWM but instead comparing the BIA with the AWM. As shown in Figure 5-6a, while the SER of the IASR after the first iteration is close to that of the BIA, the IASR after the first iteration performs slightly better because it operates one more step, low-pass filtering the reconstructed signal $\check{f}(t)$, which removes error outside the bandwidth W.

As shown in Figure 5-6a, the BIA estimates $f(t)$ much more accurate than the AWM does after the first iteration. The SER of the BIA is approximately doubled as α is twice as large; the SER of the AWM on the contrary hardly changes. For the comparison between two iterative algorithms, as α increases, both the IASR and the AWM converge faster.

As mentioned in this subsection, we provide details in analyzing the effects of α on all three algorithms. We will first focus on the analysis of the two amplitude sampling algorithms, the BIA and the IASR. However, to evaluate the simulation results, i.e. to analyze the SER, we should first distinguish what are the steps in the BIA and in the IASR that produce error. Since h is not bandlimited if f is bandlimited but not a constant, approximating h by the bandlimited-interpolation on $\{h(n\Delta)\}$ introduce aliasing. If numerical errors are not taken into account, in both algorithms the only step that introduces error is the bandlimited interpolation. Therefore, to evaluate the error on h, we only need to analyze the aliasing effect. However, to estimate the SER on f, the transformation m_α will be involved. In this case, we would like to analyze how $\|f - \check{f}\|$ relates with $\|h - \check{h}\|$. Due to the nonlinearity of the transformation m_α, it is difficult to analyze how errors relate before and after the transformation. Since h can be interpreted as a tilted and scaled version of f (as illustrated in Figure 3-1),

$\|f - \check{f}\|$ might be bounded by a finite scaling of $\|h - \check{h}\|$. Although we have not found a bound when the error is measured in L_2 norm, we will show that the parameter effects on the SER of f can be approximately evaluated by the aliasing on h.

We first show that by increasing α, aliasing effect can be reduced and thus it improves the performance of both the BIA and the IASR. One observation is that from Eq. (3.5), as α increases, h will be more similar to $-\frac{1}{\alpha}f(\frac{t}{\alpha})$, which is a bandlimited function. The aliasing effect is reduced and thus $\check{h}(y)$ gets closer to $h(y)$. The reconstructed $\check{f}(t)$ therefore gets closer to $f(t)$. This explanation can be strengthened by the exponential decay rate of the Fourier transform of h as shown in Eq. (4.10). When α is sufficiently large, the decay rate will mostly be determined by the dominating factor and thus becomes $\exp^{-|\xi|\frac{\alpha}{W}\log(\frac{\alpha}{AW})} = \frac{\alpha}{AW}^{-|\xi|\frac{\alpha}{W}}$. In this dominating factor, α appears both in the base and in the exponent. This observation shows that the tail of the Fourier transform of h decays at least as fast as $\frac{\alpha}{AW}^{-|\xi|\frac{\alpha}{W}}$. Therefore, as α increases, the signal that is outside the radiant frequency π/Δ ($\hat{f}(\xi)$ where $|\xi| > \frac{\pi}{\Delta}$) that introduces aliasing can be negligible if Δ is sufficiently small so that $\frac{\pi}{\Delta} > \xi_0$ (where ξ_0 is the same notation as in Eq. (4.11)).

However, note that there may be dependency between ξ_0 and α. If ξ_0 increases as α increases, we may need to find a smaller Δ so that $\hat{f}(\xi)$ where $|\xi| > \frac{\pi}{\Delta}$ still decays exponentially. That is, as we change α without changing Δ, the exponential decay rate $\frac{\alpha}{AW}^{-|\xi|\frac{\alpha}{W}}$ may not be able to be applied to signal outside the radiant frequency π/Δ that introduces aliasing error. Although we have not been able to show that ξ_0 does not need to increase as α increases, the following intuition suggests it. Since $h(y)$ can be thought of as a tilted function of $-\frac{1}{\alpha}f(\frac{y}{\alpha})$ with which the bandwidth $\frac{W}{\alpha}$ decreases as α increases, the increase of α intuitively might allow smaller ξ_0 rather than require larger ξ_0. Moreover, since $\frac{W}{\alpha}$ is inversely scaled with α, if Δ is sufficiently small to be able to show the signal beyond radiant frequency π/Δ decays exponentially, when α is scaled with $B > 1$, we may only need $B\Delta$ to ensure that $\check{h}(\xi)$ where $|\xi| > \frac{\pi}{(B\Delta)}$ decays exponentially. In fact, our simulation results fit well with this intuition when we fix $\frac{\alpha}{\Delta}$ but increase α as shown in Figure 5-7.

From the previous paragraph we state that the performance of the BIA and the

IASR should improve as α increases, which is consistent with the simulation results. We now discuss how much the SER can be improved when α is increased. We may want to estimate the aliasing effect by calculating the ratio of the L_2 norm of the signal to that of the signal where $|\xi| > \pi/\Delta$; this ratio will be close to the SER of h if Δ is sufficiently small[3]. Although the approximated SER can be arbitrarily close to the true SER if Δ is sufficiently small, it is still hard to estimate the approximated SER. To analyze how increasing α affects the approximated SER, not only do we need the decay rate for $\check{h}(\xi)$ where $|\xi > \frac{\pi}{\Delta}|$ remains bounded by the exponent in Eq. (4.10) as α is increased but Δ is fixed, we also need to determine how increasing α affects the coefficient C in Eq. (4.11) [4]. In order to estimate the approximated SER (the ratio of the energy of the signal to the energy of the signal where $|\xi| > \pi/\Delta$), we present a conjecture that can roughly capture the shape of the Fourier transform of h. With the shape of the Fourier transform $\hat{h}$, we can evaluate the approximated SER. Although this conjecture may need modifications to be correct, it conveys the idea that since $h(y)$ can be thought of as a tilted $-\frac{1}{\alpha}f(\frac{y}{\alpha})$, $\hat{h}$ should be similar to the Fourier transform of $-\frac{1}{\alpha}f(\frac{y}{\alpha})$.

Conjecture 5.1. *The coefficient ξ_0 in (4.11) can be chosen to be smaller than or equal to W if $\alpha > 1$. Moreover, when Δ is sufficiently small, the ratio of the L_2 norm of the signal in which $|\xi| > \frac{\pi}{\Delta}$ to the L_2 norm of the entire signal can be bounded by $\tilde{C}_0(\int_{\frac{\pi}{\Delta}}^{\infty} e^{-2|\xi|(\frac{\alpha}{W}\log(\frac{\alpha}{AW}) - \frac{\alpha - AW}{W})} d\xi)^{1/2}$ or be approximated by $\tilde{C}_1(e^{-\frac{\pi}{\Delta}(\frac{\alpha}{W}\log(\frac{\alpha}{AW}) - \frac{\alpha - AW}{W})})$ [5] where $\tilde{C}_0$ and $\tilde{C}_1$ are bounded constants independent of the parameters.*

Conjecture 5.1 states that the ratio of the L_2 norm of the signal to the L_2 norm

---

[3]It is not the same because the energy of the error calculated in the SER is $\|\sum_k \hat{h}(\xi + \frac{2\pi k}{\Delta})\|^2$ rather than $\sum_k \|\hat{h}(\xi + \frac{2\pi k}{\Delta})\|^2$. However, if the exponential decay rate is so large that the energy contained in $\hat{h}(\xi)$ where $\xi > 3\frac{\pi}{\Delta}$ is negligible, this two term can be relatively close compared to the energy of the whole signal. Dividing the energy of the signal where $\xi > \pi/Delta$ by the energy of the whole signal will be a sufficiently accurate estimation of the SER of the reconstruction of h.

[4]To give a lower bound on a ratio, we need to lower bound the numerator while upper bound the denominator. Although we wish to upper bound the denominator by the exponential decay rate, we need to be able to find the constant factor C for the exponential decay rate and evaluate how parameters affect C. Only when we can find the correspondence between C and other parameters can we analyze the parameter effects on the SER.

[5]The second approximation is trying to bound L_2 norm by L_∞ norm, which is not valid in general. However, it can be a good approximation since we only want to obtain a rough estimation on how the approximated SER scales with parameters.

of the entire signal will approximately be of the form $\tilde{C}_1(e^{\frac{\pi}{\Delta}(\frac{\alpha}{W}\log(\frac{\alpha}{AW})-\frac{\alpha-AW}{W})})$. When α is sufficiently large, it will approximately be of the form $\frac{\alpha}{AW}^{\frac{\pi}{\Delta}\frac{\alpha}{W}}$. As a result, the SER of h will approximately be of the form $20\frac{\pi}{\Delta}\frac{\alpha}{W}\log(\frac{\alpha}{AW})$. We formulate this approximation in the following conjecture.

Conjecture 5.2. *When α is sufficiently large, the SER of h will approximately be*

$$20\frac{\pi}{\Delta}\frac{\alpha}{W}\log(\frac{\alpha}{AW}) \tag{5.20}$$

with some bounded constant offset. As displayed in Figure 5-6a, as α is doubled, the value of the dark line is more than twice the value of the dashed line.

We now can approach the second estimation, the convergence rate of the IASR. Since the IASR utilizes the same bandlimited-interpolation as the BIA in each iteration, it seems that the analysis for each iteration can apply the same conjecture as Conjecture 5.2. However, it is not true because Conjecture 5.2 is based on the assumption that the amplitude-time function that will be approximated by a bandlimited interpolation is transformed from a bandlimited signal. Since the bandlimited-interpolation is taken on $e_{h,k} = h - h_k$ rather than $m_\alpha(f - f_k)$ where k is the index of the iteration, we do not know whether $e_{h,k} = h - h_k$ can be acquired from the transformation m_α from a bandlimited function and thus cannot use the conjecture anymore. We again face the same situation where we need to describe the relationships between errors before and after the transformation. As a result, there will be two parts that determine the error obtained in the next iteration. One is the change from $m_\alpha(f - f_k)$ to $e_{h,k} = h - h_k$; the other one is the bandlimited approximation of $e_{h,k}$. Since the change from $m_\alpha(f - f_k)$ to $e_{h,k} = h - h_k$ is determined by how m_α operates on f and f_k, intuitively if m_α will not tilt either f or f_k too much, there will be little difference between $m_\alpha(f - f_k)$ and $e_{h,k}$. We know when α is sufficiently greater than the largest negative derivative, h will have a similar shape as f. Therefore, the convergence rate may mostly depend on α and AW.

Here we evaluate the effect of α on the performance of the AWM. The first observation is that as α increases, since h gets closer to $-\frac{1}{\alpha}f(\frac{t}{\alpha})$, the nonuniform samples

are more uniformly distributed. A rigorous way to show it is by Eq. (5.17). Since Δ is fixed and $f'(\eta_n)$ is bounded, as α increases, the right hand side of Eq. (5.17) tends to be $\frac{\Delta}{\alpha}$ and depends less and less on f.

Moreover, from Eq. (5.17), $\delta = \sup\{t_{n+1} - t_n\}$ is approximately inversely proportional to α. By Theorem 2.7, since the error bound is proportional to $(\frac{\delta W}{\pi})^k$ where k is the index of the iteration, the SER will be greater than or equal to $20k \log(\frac{\pi}{\delta W})$. This factor can be approximated by $20k \log(\frac{\alpha \pi}{\Delta W})$. In comparison with Conjecture 5.2, when α is scaled with $B > 1$, the SER of the BIA is scaled more than B times while the SER obtained after each iteration of the AWM increases by $20 \log B$. This benefit attained from the BIA does not consider the advantage of using the BIA over the AWM in the first iteration only, since the latter is merely a zero order hold approximation. We can say more: as α is scaled with B, the number of iterations for the AWM to reach the same SER as of the BIA may be more than $1/B$ times as before α is scaled.

With the SER of the AWM over iterations, we can also analyze the slope of the SER. The slope of the SER of the AWM, which is bounded by $20 \log(\frac{\pi}{\delta W})$, can be approximated by $20 \log(\frac{\alpha \pi}{\Delta W})$. Although the convergence rate r of the AWM decreases (where r is defined as in the footnote in Section 2.2) as α increases, the first guess is hardly affected since the first guess is a zero order hold approximation. Moreover, the AWM converges much more slowly than our method. It is because the larger α is, the more we can gain from the exponential decay rate of the Fourier transform of h. Therefore, since we know more about the samples than merely the fact that they are nonuniformly distributed when mapped to the time domain, we can utilize this knowledge to outperform the AWM.

We should emphasize that although all these conjectures are not rigorous and are likely to be incorrect, they are important for future research directions and providing intuitions. Moreover, with all these discussions, it is clear where the difficulty of analyzing the BIA and the IASR algorithms is. We state the two most important unsolved problems in analyzing the SER of the BIA and the IASR: one is to find a more precise description of the shape of $\hat{h}(\xi)$ than having an exponential decay; the

other one is to find the L_2 errors relationship before and after the transformation. In the following discussion, we will come back to conjectures discussed in this section and utilize them to analyze other parameter effects.

5.4.1.2 Change of Δ

To test the effect of Δ, we decrease the sampling rate from $1/20$ to $1/10$. As shown in Figure 5-6b, the SER of the BIA is approximately doubled as Δ is scaled by a half. This can be explained by Conjecture 5.2. The IASR still converges much faster than the AWM. Moreover, the rate of the convergence of the IASR seems to be relatively invariant to the change of Δ. This observation will be more apparent when we discuss the case when AW is very close to α in Section 5.4.2.3. On the other hand, the simulated convergence rate of the AWM still follows the theoretical rate $\frac{\delta W}{\pi}$. Thus the slope of its SER $s = 20 \log(\frac{\pi}{\delta W})$ as discussed in Section 5.4.1.1 decreases as Δ is doubled, since Δ/α approximately equals to δ.

While nearly all the observations are similar to observations when α is increased, one interesting difference is the effect of Δ on the convergence rate of the IASR. As discussed in Section 5.4.1.1, the convergence rate of the IASR will be determined by how errors are related before and after the transformation m_α and also by the bandlimitedness of the error $e_{h,k}$. This might be more related with how tilted h and h_k can be (where k is the index of the iteration), which is mostly determined by α, W, and A. Therefore, in the simulation result, the convergence rate seems to be invariant to the change of Δ. Another explanation is that the error $e_{h,k} = h - h_k$ might become really close to a bandlimited function after the first iteration and thus as long as Δ is sufficiently small, the slope of the SER will be invariant to Δ and be more relevant to A, W, and α.

5.4.1.3 Change of W

To understand the effect of the bandwidth, W is increased from 16π to 32π. Figure 5-6c shows that as W is decreased by a half, the SER of the BIA approximately doubles. It can be explained by Conjecture 5.2. We should recall that in Section 5.3.1, the

63

randomly generated signals will be scaled in amplitude accordingly to the change of bandwidth W to ensure the first derivative of f is smaller than one. Therefore, AW in Eq. (5.20) is fixed and the SER will approximately be inversely proportional to W. The simulated convergence rate of the AWM follows the theoretical rate $r = \frac{\delta W}{\pi}$ and therefore the slope of its SER $20 \log(\frac{\pi}{\delta W})$ still decreases by the same factor as in the case of α and Δ. The simulated SER of the IASR also converges faster as W is decreased. It satisfies our intuition that as W increased, $\frac{\alpha}{AW}$ gets closer to 1 and thus h will be more tilted. Therefore, $m_\alpha(f - f_k)$ will be more different from $h - h_k$.

5.4.1.4 Fix α/Δ with a change of α

Besides changing one of the three parameters at a time, we also consider fixing the average nonuniform sampling rate. That is, we fix α/Δ while increasing α. The simulation results are shown in Figure 5-7. Here α and Δ are increased by a factor of 4 simultaneously; thus the modified parameter settings are $\alpha = 16$ and $\Delta = 1/5$.

As shown in Figure 5-7, the SER of the BIA hardly improves as α increases. This is slightly different from the implication of our conjecture. It suggests that either the conjecture needs some modification or $\frac{\pi}{\Delta}$ is no longer greater than ξ_0. For the AWM, the convergence rate hardly changes. This follows the theoretical bound since δ is approximately unchanged. From Eq. (5.17), when $\frac{\alpha}{\Delta}$ is fixed and α is increased, the negative term would be smaller and thus the corresponding nonuniform samples will be more uniformly distributed; this however hardly affects the simulated convergence rate of the AWM which is still dominated by the average nonuniform sampling rate of f. On the contrary, as α increases, the IASR converges faster. As we discussed in Section 5.4.1.1 on the relationship between Δ and α so that the out-of-band signal ($\check{h}(\xi)$ where $|\xi| > \frac{\pi}{\Delta}$) has exponential decay, we predict that when α becomes $B\alpha$ we may only need $B\Delta$ to ensure that the out-of-band signal decays exponentially. This is supported by the simulation result. Also, as we mention in Section 5.4.1.2, the IASR is relatively invariant to any change of Δ as long as Δ is sufficiently small. This conjecture is supported by the simulation result as well since the IASR can converge faster when α is increased.
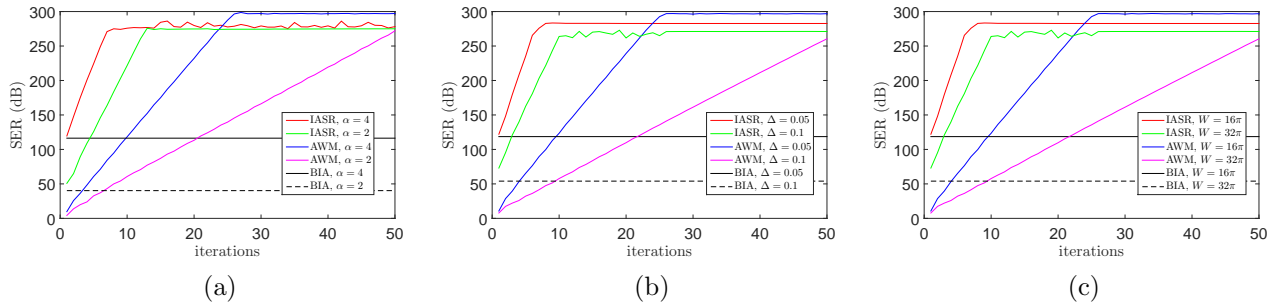
Figure 5-6: Comparison among three reconstruction algorithms (IASR, AWM, BIA) based on changing a single parameter – (a) α, (b) Δ, (c) W.
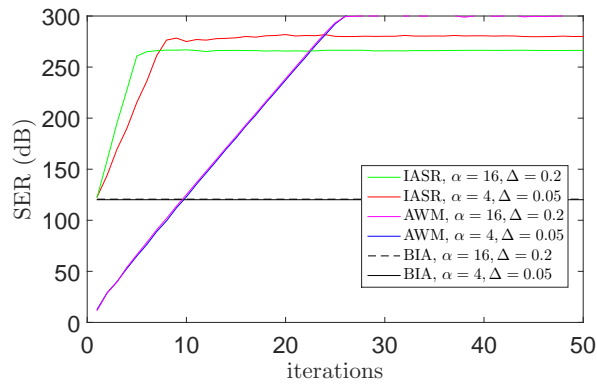
Figure 5-7: Comparison among three reconstruction algorithms when average sampling rate in time is fixed but α is increased

5.4.1.5   Variance Analysis and Numerical Error

In order to test the robustness of our algorithms, we also simulate our methods 100 times on randomly generated signals with the default parameter settings ($\alpha = 4$, $\Delta = 1/20$, $W = 16\pi$). Its mean and two standard deviations are calculated as shown in Figure 5-8. We can see that although the standard deviation of the SER of the IASR is greater than that of the the AWM, every SER value within the confidence interval of the IASR is much larger than the value within the confidence interval of the AWM. Moreover, this standard deviation may be due to the numerical errors from the realizations of m_α and $m_{1/\alpha}$. These errors are not produced in the simulation of the AWM, since the AWM only involves one transformation, which is performed when the nonuniform samples are mapped from $h(n\Delta)$. Moreover, in our implementation each $f(t_n)$ is not calculated by $-\alpha h(n\Delta)$ but directly by $f(t_n) = f(h(n\Delta) + \frac{1}{\alpha}n\Delta)$.

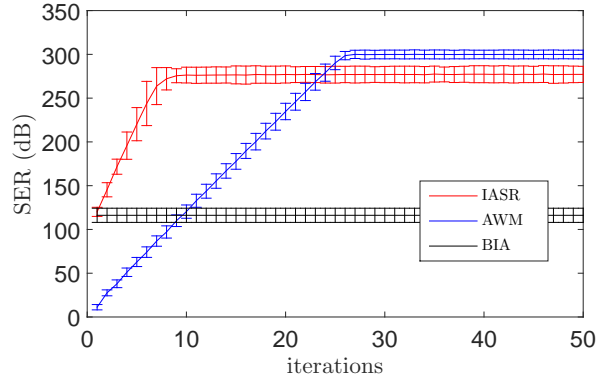Figure 5-8: Robustness comparison among three reconstruction algorithms

The difference between these two implementations is that the samples $h(n\Delta)$ would suffer numerical error from the linear interpolation while f will not. With the latter implementation, the nonuniform samples $\{(t_n, f(t_n))\}$ only encounter numerical errors from the timing $\{t_n\}$ [6], rather than from a noisy f. This explains why in our simulation results, when algorithms converge, the AWM would obtain higher SER. Although the IASR does not attain the same SER as the AWM does, by applying Theorem 2.5 to our simulation results, since the Beurling lower density $D_-(\{t_n\}) = \Delta/\alpha$ is taken to be larger than twice the bandwidth, the reconstructed signal is ensured to be extremely close to the original signal if the numerical error is sufficiently small.

5.4.2 Deterministic sinusoidal functions

In this subsection, we simulate deterministic signals with only one harmonic. Simulating deterministic functions is important for worst case analysis. As shown in Figure 4-3 and discussed in Section 4.3, when A and W are fixed, the Fourier transform of h will decay slowlier when f consists of more high-frequency components. It intuitively suggests that the Fourier transform of the amplitude-time function corresponding to $f(t) = A\sin(Wt)$ may decay the slowliest among all other f with the same maximum amplitude and bandwidth. Although it is not proved, it is reasonable since in

---

[6]The value t_n may not be equal to the true $h(n\Delta) + \frac{n\Delta}{\alpha}$ since h contains numerical errors. However, since the uniformly sampled value is obtained by directly calculating $f(t_n)$, $(t_n, f(t_n))$ is really a sample point on the plot of f.

such case the maximum negative derivative will be AW and thus reaches the bound provided by Bernstein's inequality as shown in Eq. (4.2), by which we develop the exponential decay rate of $\hat{h}(\xi)$. Thus, to better understand how parameters can affect our proposed algorithms when the bound for the Fourier transform decay rate is tight, these single harmonic sinusoidal functions are simulated to test our algorithms.

Besides the three parameters α, Δ, and W, we also compare three algorithms in the situation when W is changed but the corresponding h is the same except with a different amplitude scaling. This effect is discussed in Section 3.2.2. Moreover, in order to understand when our algorithms outperform the AWM and also the weakness of our algorithms, we design our tested signals and parameters so that the magnitude of the maximum negative first derivative of f is close to α.

We set the input signal $f(t) = \sin(2\pi t)/8 + 2t$ as the reference signal in Figure 5-12, 5-9, and 5-11 with the same $\Delta = 1/20$ so that the parameter effects can be analyzed by comparing the performance after changing some parameters with this default setting. Since in these simulations, $\frac{\alpha}{AW}$ is not large, the conjecture may not be able to be used [7]. In this subsection, we will therefore not use the conjecture but will rather indicate important discoveries from simulation results and provide reasonable explanations.

5.4.2.1   Change of α and Δ

As discussed in Section 5.4.1, when only α or Δ is changed, the effects of these parameters are similar to those when signals are randomly generated. In Figure 5-9a, α is changed to be 4 and in Figure 5-9b Δ is changed to be $1/10$.

As α is doubled, the SER of the BIA is more than twice as large, and as Δ decreases, the SER of the BIA is scaled with similar factor as with $\frac{1}{\Delta}$. This observation is consistent with the the simulated result when the signal is randomly generated as shown in Figure 5-6b. Moreover, the IASR converges faster as α increases and the convergence rate is relatively invariant to the change of Δ. These two results also

---

[7]The conjecture requires large decay rate of the Fourier transform; when $\frac{\alpha}{AW}$ is not large, the decay rate will not be sufficiently large for the conjecture to be applied.
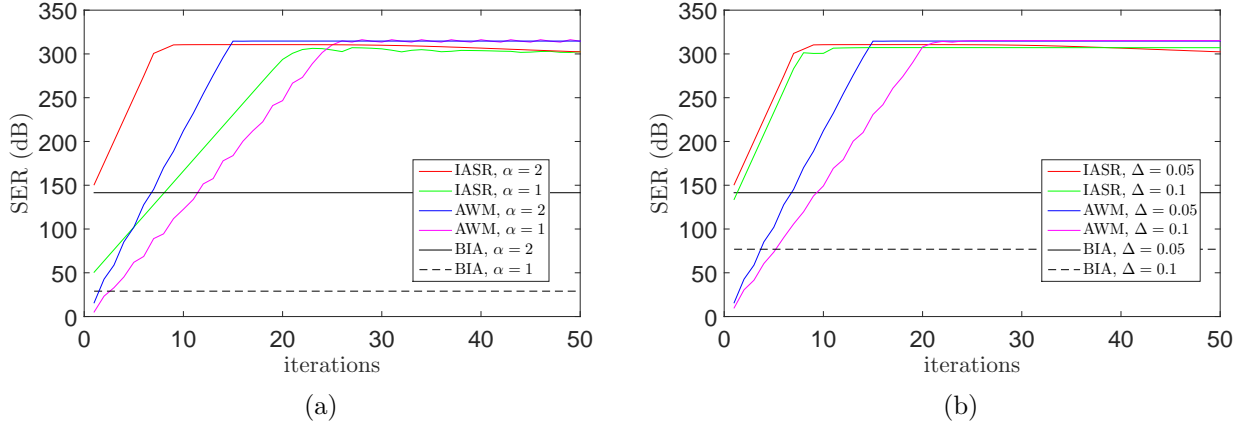
Figure 5-9: Comparison based on deterministic sinusoidal signals based on changing a single parameter – (a) α, (b) Δ

are the same as when input signals are randomly generated. One more interesting observation is that although we mention that the simulation result of the BIA should be similar to that of the first iteration of the IASR, it is not the case when $\Delta = 0.1$ as shown in Figure 5-9b. The observation suggests that adding a low-pass filter sometimes will be useful in enhancing the performance of the BIA.

5.4.2.2   Change of W and A

We also discuss the situation when the bandwidth W is doubled. However, while the amplitude of randomly generated functions as discussed in Section 5.3.1 will be normalized with respect to a change of bandwidth so that the maximum absolute value of the first derivative of the input function is smaller than one, it is not the case in Figure 5-10a. The tested function corresponding to the green, purple, and dashed black lines is $\sin(4\pi t)/8 + 2t$ without any normalization. As a result, the size of the parameter AW is affected. When $\frac{\alpha}{AW}$ gets closer to 1, both the SER of the BIA and the convergence rate of the IASR become worse and get closer to the corresponding performance of the AWM.

We also would like to experiment on settings in which $\frac{\alpha}{AW}$ approaches 1 but instead by changing A; that is, the tested signal becomes $\sin(2\pi t)/4 + 2t$. This simulation result is shown in Figure 5-10b. In this case, the BIA performs better

68

when A is increased than when W is increased while AW is the same. However, the convergence rate of the IASR does not seem to change when AW is fixed. The IASR converges more slowly when AW is increased. On the contrary, the convergence rate of the AWM is relatively invariant to changing A. Therefore, the AWM can converge faster than the IASR when A is increased as in Figure 5-10b.

While the AWM still can be explained by its theoretical convergence rate r, here we explain the performance of the BIA and the IASR by two equations. First, if $\frac{\alpha}{AW}$ is much greater than 1, i.e. $\frac{\alpha}{W} \gg A$, then by (4.10), we can obtain the following:

$$
\begin{aligned}
\sigma &= \frac{\alpha}{W} \log(\frac{\alpha}{AW}) - \frac{\alpha - AW}{W} \\
&= \frac{\alpha}{W} \log(\frac{\alpha}{AWe}) + A \\
&\approx \frac{\alpha}{W} \log(\frac{\alpha}{AWe}) \\
&= A\frac{\alpha}{AW} \log(\frac{\alpha}{AWe}).
\end{aligned}
\tag{5.21}
$$

From Eq. (5.21) we observe that the BIA should perform better when A is increased than W is increased when A and W are increased by the same factor respectively [8]. In cases where $\frac{\alpha}{AW} \simeq 1$, from Eq. (4.12), we still can observe that it is better to increase A than W. However, since the convergence rate of the AWM does not depend on A, changing A hardly affects the performance of the AWM. Therefore, our algorithm may converge slowlier than the AWM when $\frac{\alpha}{AW} \approx 1$ and W is small. Conversely, when $\frac{\alpha}{AW} \approx 1$ but W is large, we may still consider to use the IASR algorithm. It is because the convergence rate r of the AWM is proportional to W, although the IASR will converge slowlier as well when W is increased, the performance of the first iteration is much better than that of the AWM. This suggestion will be strengthened in Section 5.4.2.3.

In fact, there is an interesting interpretation of how A and W affect amplitude sampling when AW is fixed. This interpretation can be observed from Eq. (3.13).

---

[8]This statement introduces the same ambiguity as discussed in Subsubsection 5.4.1.1 about the dependence of ξ_0 in Eq. (4.11) on parameters A and W. As discussed in Subsubsection 5.4.1.1, we assume that Δ is sufficiently small so that $\frac{\pi}{\Delta}$ remains to be greater than ξ_0 when parameters are changed; the ambiguity can be resolved.
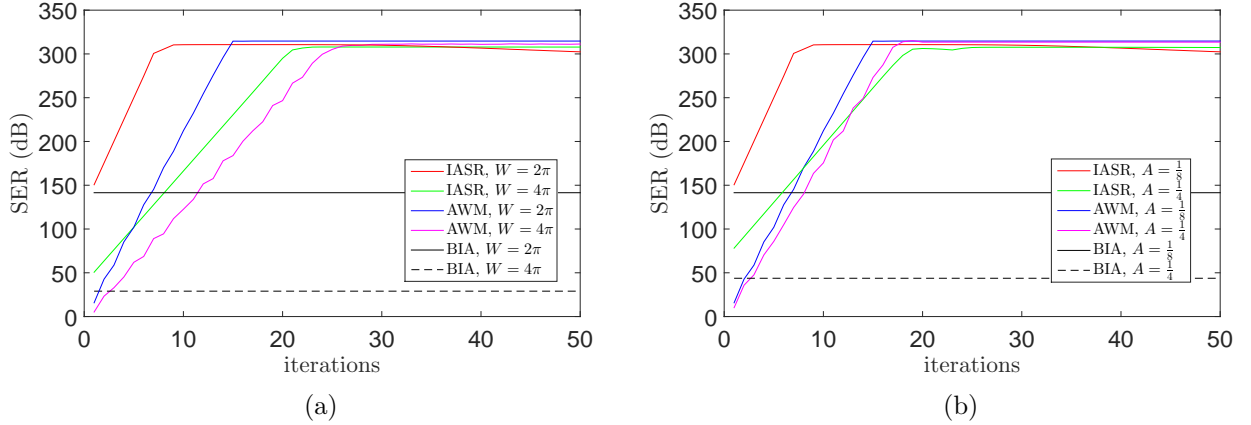
Figure 5-10: Comparison based on deterministic sinusoidal signals based on changing a single parameter – (a) W, (b) the amplitude A

If we denote the amplitude-time function corresponding to the tested signal whose SER is indicated by the green line in Figure 5-10a as $h_1(y)$ and that in Figure 5-10b as $h_2(y)$, from Eq. (3.13) we know $h_1(y) = h_2(2y)$. That is, the algorithms in fact are reconstructing the original signal based on samples from the same amplitude-time function except that $h_1(y)$ which corresponds to f with a larger W varies twice as fast as h_2 and therefore expands twice as much as h_2 does in frequency domain. This observation explains why the convergence rates of the IASR are similar when AW is fixed while the SER after the first iteration when A is increased is larger than when W is increased.

We also discuss the situation when the average sampling rate of f remains the same but with different α as in the random input signal cases. The simulation results can be explained as in Section 5.4.1.4 and are shown in Figure 5-11. It once again supports that when α is increased by a factor $B > 1$, the SER of the IASR after the first iteration can almost be achieved by also scaling Δ by B; that is, we can reduce the sampling rate in the amplitude domain when α is increased (or keep the average sampling rate in the time domain). Moreover, the convergence rate of the IASR depends more on α than on Δ. Therefore, with $\frac{\alpha}{\Delta}$ fixed, we can enhance the performance of the IASR by increasing α.

We next perform experiments on the performance of the BIA and the IASR when

70
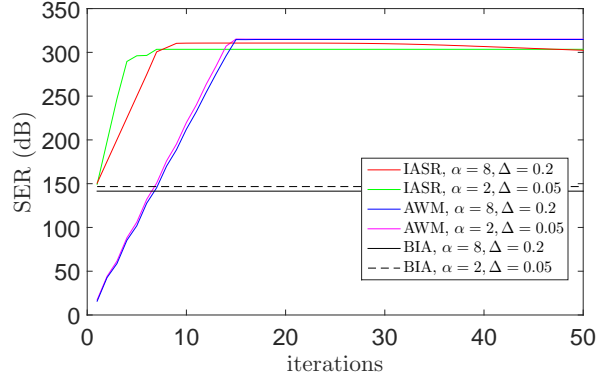
Figure 5-11: Comparison based on deterministic sinusoidal signals when average sampling rate in time is fixed but α is increased
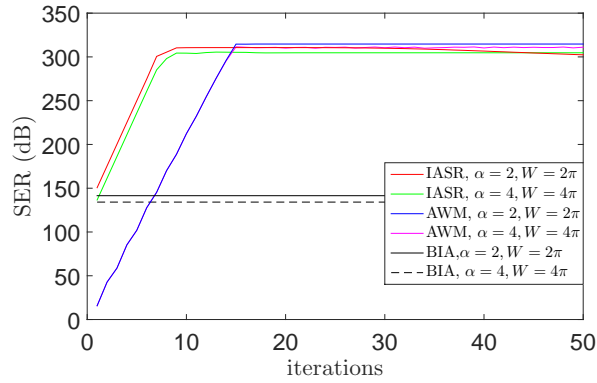
Figure 5-12: Comparison based on deterministic sinusoidal signals with the same amplitude-time function but different scaling in amplitude

the amplitude-time functions are the same but with different amplitude scaling. The simulation result is shown in Figure 5-12 where the compared signal is chosen to be $\sin(4\pi t)/8 + 4t$. By Eq. (3.12), it is easy to check that its corresponding amplitude-time function is half-sized of the original amplitude-time function. The simulation result reveals that the performance of all three algorithms hardly changes.

5.4.2.3 Effect of $\frac{\alpha}{AW}$

So far we have discussed simulation results when parameters are changed as in the setup of randomly generated input signals. However, as discussed in Section 5.4.2.2, a factor that dominates our performance is how close $\frac{\alpha}{AW}$ is to 1. This statement can also be understood from Eq. (4.12). When $\frac{\alpha}{AW} \to 1$, the inequality in Eq. (4.12) will

be closer to an equality; since the right hand side is a quadratic function, it will goes to 0 approximately quadratically fast as $\frac{\alpha}{AW} \to 1$. In other words, the exponential decay rate will be so small that the Fourier transform of h will act like a constant. In this case, the aliasing effect from the signal where $|\xi| > \pi/\Delta$ cannot be neglected if Δ is not sufficiently small and therefore the bandlimited-interpolation approximation $\check{h}(y)$ will be much different from $h(y)$.

We also would like to understand how the AWM performs when δ approaches $\frac{\pi}{W}$. In Section 5.3.4, Eq. (5.19) requires the sampling rate on the amplitude-time function h to be twice as fast as the Nyquist rate to guarantee the validity of the AWM. This requirement is due to the negative term $-(f'(\eta_n))$ in Eq. (5.17). The higher the negative derivative is, the more positive this term is and thus the tighter the requirement in Eq. (5.19) is. The constraints on Theorem (2.7) cannot be guaranteed if Δ is not sufficiently small.

From the above discussion, it suggests that the closer the largest magnitude of the negative derivative is to α, the worse both the IASR and the AWM will perform. This suggestion fits our intuition as well, since the closer the negative derivative $f'(t_0)$ is to α, the smoother $g(t) = f(t) + \alpha t$ is around t_0, and the sharper $h(y)$ will be around $y = f(t_0) + \alpha t_0$. On one hand, the sharper a function is, the larger high frequency components are and the more different a bandlimited-interpolation approximation $\check{h}$ is from h. On the other hand, the sharper h is around a certain timing, the fewer sampling points can be obtained around that timing, and thus the greater distance nonuniform samples are from their uniform counterparts.

To understand how $\frac{\alpha}{AW}$ affects both our methods and the AWM, we keep $\frac{\alpha}{AW}$ to be close to 1 and test their performance with respect to different Δ and different W. As shown in Figure 5-13, the input signal is fixed to be $\sin(2\pi t)/8 + t$ and Δ is increased as follows: $\{0.05, 0.1, 0.2, 0.25\}$. In this case, $\frac{\alpha}{AW} = \frac{1}{\pi/4} \approx 1.273$ which is close to 1. The green, purple, and dashed lines indicate the settings when $\Delta = 0.25$. In Figure 5-14, we fix $\frac{\alpha}{AW}$ by choosing two functions $f_1(t) = 4\sin(2\pi t)/8 + 4t$ as the red, blue, and dark lines indicate, and $f_2(t) = \sin(8\pi t)/8 + 4t$ as the green, purple, and dashed lines indicate. In this case, $\frac{4}{\pi} \approx 1.273$ is close to 1. The parameter Δ is

72

chosen to be 0.05.

In Figure 5-13, when Δ changes from 0.05 to 0.2, the IASR seems relatively invariant to the change compared to the AWM. This is similar to the observation in Section 5.4.1.2. However, when $\Delta = 0.25$, the IASR fails to converge while the AWM still can converge and recover the original signal. Since our tested signal is $\sin(2\pi t)/8$, we only require more than two sample points to uniquely represent the signal. This is satisfied in our simulation since there are 4 sample points. This simulation result implies that either subtle numerical error will affect the convergence of the IASR when $\frac{\alpha}{AW}$ is approximately 1, or that the unique representation of f from samples of h may not be sufficient for the IASR to converge. Although it is difficult to theoretically find the constraints for the IASR to converge[9], when it does and when α is carefully chosen, the IASR converges more and more faster than the AWM does as Δ increases since the convergence rate of the IASR is relatively invariant to the change of Δ while the convergence rate[10] r of the AWM as shown in Theorem 2.7 is approximately proportional to Δ.

We now analyze the effects of A and W when $\frac{\alpha}{AW}$ is fixed and is close to 1. As revealed in Figure 5-14, the simulation results can also be explained as in Section 5.4.2.2. In Section 5.4.2.2, we mention that the performance of both the IASR and the AWM increases when A increases (or W decreases) and AW is fixed. However, when AW is fixed, the convergence rate of the IASR does not seem to change while the convergence rate r of the AWM is proportional to W. As discussed in Section 5.4.2.2, the former phenomenon can be explained by Eq. (3.13) that when AW is fixed, the corresponding $h(y)$ is scaled in the variable y in proportional to the scaling factor of W. The simulation results suggest that when the input function is fixed and its time and amplitude scale inversely proportionally to each other, the convergence rate of the IASR may not change. We should notice that it is not the case as in

---

[9]In most cases where one can show the convergence of an algorithm, the convergence rate can also be found. However, as discussed in Subsubsection 5.4.1.1, we show the difficulty of analyzing the error generated from the bandlimited-approximation for each iteration and the difficulty of analyzing the relationship between errors before and after the transformation m_α. Both are crucial for finding conditions for the IASR to converge.

[10]The definition of the convergence rate is the same as the footnote in Section 2.2 described
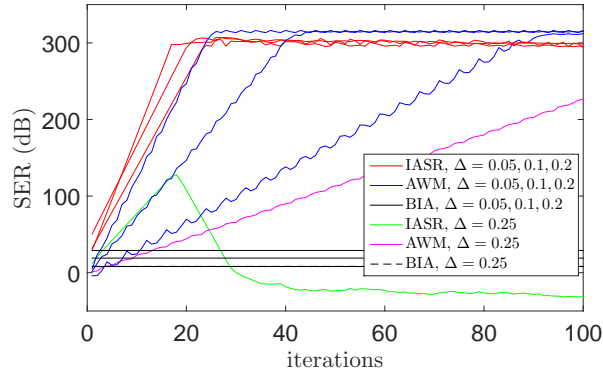
Figure 5-13: $A * W$ is fixed but Δ is changed.

Figure 5-6c where the input function is not fixed. This difference indicates that the convergence rate of the IASR may require more careful analysis and may depend more than just on A, W, and α. The slope of the SER of the AWM as shwon in Figure 5-14 follows Theorem 2.7 which indicates that the slope of the SER should be $20 \log(\frac{\pi}{\delta W})$ and will increase by $20 \log B$ if W is scaled with $\frac{1}{B}$.

As a result, while it is true that both the IASR and the AWM perform better when W is smaller, the convergence rate of the IASR does not change correspondingly with W while the convergence rate of the AWM is proportional to W. Therefore, two statements can be made. Since our convergence rate is relatively more invariant to the change of W when AW is fixed, when W becomes larger, the IASR performs better than the AWM. On the other hand, when W is smaller, although our IASR may not converge as fast as the AWM does, since the approximation obtained after the first iteration is more accurate, the convergence rate may not matter.

5.5 Simulation Results Summary and Amplitude Sampling Parameter Design

In this section, we summarize the parameter effects on all three algorithms (the BIA, the IASR, and the AWM) as discussed in Section 5.4. We will first discuss the reason why the IASR generally converges within fewer iterations than the AWM does. With this knowledge, it is natural to understand what may be a range of parameter
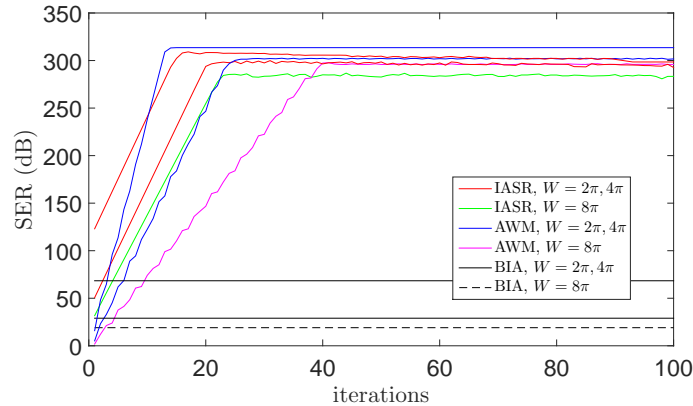
74

Figure 5-14: $A * W$ is fixed but W is changed.

settings in which our algorithms are limited. We then explore parameter settings in which our proposed algorithms cannot approximate well the original signal; we will also discuss settings where under amplitude sampling the performance of the AWM may be limited. It turns out that all three algorithms are restricted under the same parameter settings where $\frac{\alpha}{AW}$ is close to 1. However, since α is a parameter we can choose, we can avoid such settings. We then show that with the assumption that $\frac{\alpha}{AW}$ is not close to 1, there are two differences between the main factor that affects the performance of our algorithms and the factor that determines the performance of the AWM. Namely, one is the effect of Δ; the other one is the effect of A. We will then show how we can utilize these two differences to design parameters Δ, α, and A (by scaling f) so that our algorithms (the IASR in particular) can outperform the AWM and can well recover the original signal.

The main reason that enables the IASR to generally perform much better than the AWM in both the accuracy of the first approximation and the convergence rate is that it is designed based on the amplitude sampling settings. That is, $\{h(n\Delta)\}$ are not uniform samples from any signal but instead from a more structural signal that has many nice properties as presented in Chapter 3 and Chapter 4. Specifically, with the knowledge of the exponentially decaying Fourier transform of h, we know that a bandlimited-interpolation approximation of h based on sufficiently dense samples will introduce little error. Therefore, as shown in Section 5.4, the SER obtained after the

75

first iteration of the IASR which takes advantage of this knowledge is much larger than that of the AWM which only approximates the nonuniform samples by zero order hold approximation.

As discussed above, our algorithms are designed based on the assumption that h is close to a bandlimited function and thus aliasing effect introduced by the bandlimited-interpolation can be negligible or can be removed after few iterations. Therefore, it is important to analyze the decay rate of the Fourier transform of h in order to evaluate the performance of our proposed algorithms. As shown in Section 5.4, we use (4.10) to develop two conjectures on evaluating the SER of the BIA. These conjectures are helpful in analyzing the performance of the BIA when input signals are randomly generated. Moreover, the upper bound of the exponential decay rate as indicated in (4.12) implies that one important factor that affects the exponential decay rate is $\frac{\alpha}{AW}$. Therefore, we also explore the performance of our algorithms when the exponentially decay rate bound is tight by testing the algorithms on reconstructing specific sinusoidal functions so that $\frac{\alpha}{AW}$ is slightly greater than 1. Interestingly, $\frac{\alpha}{AW}$ is also related with the convergence rate of the IASR. As discussed in Subsubsection 5.4.1.1, the convergence rate of the IASR may be more closely related to how much the m_α transformation tilts f, which is determined by the difference between α and $f'(t)$. Since $f'(t)$ can be bounded by AW by Bernstein's inequality, the convergence rate of the IASR will be more related with the factor $\frac{\alpha}{AW}$ than Δ. From most of the simulation results, as $\frac{\alpha}{AW}$ becomes larger, the IASR converges faster and is relatively invariant to Δ as long as Δ is not really close to the required average sampling rate.

The performance of the AWM, on the other hand, depends mostly on the average sampling rate. Since we map the uniform samples $h(n\Delta)$ back to nonuniform samples on f, the sampling rate on f will be α times the sampling rate of h. Therefore, the most important factor that dominates the convergence rate of the AWM is $\frac{\alpha}{W\Delta}$, which is obtained by replacing δ in the convergence rate shown in Theorem 2.7 with $\frac{\Delta}{\alpha}$. We notice that δ is defined as the supreme of the time difference of nonuniform samples. From (5.17), we notice that when α is much larger than $f'(t)$, δ can be approximated by $\frac{\Delta}{\alpha}$, which validates our replacement mentioned above. However, when $\alpha + f'(t)$ is

76

close to 0, δ will be extremely large and will be much different from $\frac{\Delta}{\alpha}$. The AWM may still converge to the right function but we can no longer utilize Theorem 2.7. Moreover, as discussed in Section 2.1, the robustness of nonuniform sampling depends on the deviation of nonuniform samples to their uniform counterparts. Therefore, when $\alpha + f'(t)$ is close to 0, the AWM may encounter a robustness problem. As mentioned in the last paragraph, we can bound $f'(t)$ by Bernstein's inequality with AW. Whether $\alpha + f'(t)$ is close to 0 can be estimated by evaluating the closeness of $\frac{\alpha}{AW}$ to 1. Therefore $\frac{\alpha}{AW}$ should also not be close to 1 when we want to use the AWM to reconstruct signals based on the amplitude sampling settings.

As discussed in the last two paragraphs, α should not be chosen too close to AW for both our algorithms or the AWM. We now compare the parameter effects on our algorithms and on the AWM under the assumption that $\frac{\alpha}{AW}$ is not close to 1. From the last two paragraphs and also from the discussion in Section 5.4, we notice two main differences of the parameter effects on our IASR and the AWM. To begin with, there is no Δ parameter in the factor $\frac{\alpha}{AW}$ that mostly determines the rate of convergence of the IASR. Moreover, there is no A in the dominated factor $\frac{\alpha}{W\Delta}$ of the AWM. These two main differences have played important roles in the simulation results in Section 5.4.

As a result, we can utilize these two differences to design amplitude sampling. The main reason why there is no Δ factor in the analysis of the convergence rate of the IASR is based on the assumption that $\frac{\alpha}{AW}$ is not close to 1 and that the average sampling rate is slightly larger than the required sampling rate for a unique representation. From Figure 5-6b and Figure 5-11, once these assumptions are satisfied, then the IASR algorithm can converge much and much faster than the AWM does when Δ increases. That is, we may not need small Δ to achieve a desired reconstruction convergence rate. This benefit can also be observed when the sampling rate of the nonuniform samples is fixed. That is, when $\frac{\alpha}{\Delta}$ is fixed, the performance of our algorithm will still enhance as α increases, while the performance of the AWM hardly changes. On the other hand, although decreasing Δ will not decrease the convergence rate of the IASR as much as that of the AWM, since the SER of the BIA will

approximately be scaled inversely proportional to Δ, the IASR may still be able to converge to the original function with fewer iterations than the AWM does.

We now focus on the other main difference between our algorithms and the AWM, the effect of AW. While our algorithms will be affected by W and AW, i.e. the amplitude plays a role, it is not the case for the AWM. If for some applications the amplitude of f is not a concern or is already known, then we can either scale our input signal or increase α to compensate the size of the bandwidth W. This benefit cannot be attained from the AWM, whose convergence rate is determined by W and not by A. This benefit can be observed from Figure 5-14 and also from subfigure 5-6c, when we fix AW and scale the tested signal correspondingly with respect to the bandwidth W. We notice that the convergence rate of the IASR is relatively invariant to the bandwidth W when AW is fixed.

Chapter 6

Conclusion and Future Directions

In this thesis, we study a recently proposed framework, amplitude sampling [11], which represents a signal through a time sequence rather than an amplitude sequence as in the case with conventional sampling methods. Unlike level-crossing sampling, which also represents a signal by a time sequence, amplitude sampling maps a bandlimited function uniquely to an amplitude-time function by an amplitude-time transformation m_α and thus can preserve the information contained in the bandlimited function and can achieve any required sampling density as shown in Eq. (5.3). As a result, it is likely to develop an exact reconstruction algorithm under amplitude sampling, which is the objective of this thesis. In order to design an algorithm that can reconstruct the original signal from samples of its amplitude-time function, we analyze the time-domain properties and frequency-domain properties of amplitude-time functions in Chapter 3 and Chapter 4. An iterative algorithm for the implementation of the transformation m_α is also proposed in Chapter 3.

With time-domain properties and frequency domain properties of amplitude-time functions and the ability to implement m_α, the bandlimited-interpolation approximation (BIA) algorithm and the iterative amplitude sampling reconstruction (IASR) algorithm are developed and the comparison among these two methods and a nonuniform sampling reconstruction algorithm, the adaptive weights method (AWM) are analyzed based on different parameter settings in Chapter 5. Simulations show that the SER of the BIA is much greater than the SER of the AWM after the first iteration.

The IASR on the other hand generally converges and the number of iterations needed is in general much smaller than that needed by the AWM. Moreover, two differences in parameter effects on the convergence rate of the IASR and on the convergence rate of the AWM are presented: the effect of Δ and the effect of A. The first observation indicates that in most cases the IASR does not need as high sampling rate as that for the AWM to attain the same convergence rate. Moreover, the IASR can converge faster by increasing α but fixing the nonuniform sampling rate. The other observation shows that the convergence rate of the IASR can be increased by shrinking the maximum amplitude of the amplitude-time functions. That is, the IASR can converge faster with smaller maximum amplitude while the convergence rate of the AWM hardly depends on the size of the A. With this observation, the IASR is able to converge much faster than the AWM does when a function with high bandwidth is encountered.

6.1   Future Directions

In this section, we discuss some possible future research directions. There are two main unsolved problems in this thesis. The first is to prove the convergence of the IASR and add conditions if needed. The other is to analyze rigourously the parameter effects on both the BIA and the IASR. We will suggest possible directions to solve these problems. We will also discuss one interesting research direction: the correctness of α. Other interesting topics are outlined in the last paragraph of this section.

As mentioned above, we have not yet proved the convergence of the IASR, although in simulations it generally can converge and we have shown that as long as it does converge it converges to the right function. However, since there is one case in our simulations where $\Delta \approx \frac{\pi}{\alpha W}$ and the IASR fails to converge, we will need to carefully reduce numerical errors to understand whether it is because when the sampling rate is close to the required sampling rate for a unique reconstruction the simulated performance of the IASR will be sensitive to numerical errors, or because more conditions are needed to prove the convergence of the IASR besides the sampling rate

larger than that required for uniqueness. As discussed in Section 5.2, we cannot utilize methodologies of proving the convergence of iterative nonuniform sampling algorithms to prove the convergence of the IASR. Therefore, a possible way to prove the convergence is to directly use a more generalized theorem: the Banach fixed-point theorem. By which if we can show $\|f_{k+1} - f_k\| < \gamma\|f_k - f_{k-1}\|$ where $\gamma < 1$, then the IASR will have geometric convergence. However, while we do not know much about the L_1 norm of the D/C converter and the low-pass filter but can measure their L_2 norm, we do not know the L_2 norm of the transformation m_α. That is, we would hope to analyze how $\|f_{k+1} - f_k\|$ relates with $\|h_{k+1} - h_k\|$ in the L_2 norm. We have already pointed out in Subsubsection 5.4.1.1 the importance of analyzing this relationship since it is also crucial for estimating the convergence rate of the IASR. It is reasonable since in order to prove the Banach fixed-point theorem we will need γ, while with γ we also obtain a convergence rate. As a result, the relationship between errors before and after the transformation m_α becomes one of the most important future research directions for amplitude sampling.

Another unsolved problem is to estimate the parameter effects on the SNR of the BIA and on the convergence rate of the IASR. To estimate the former, we would like to modify conjectures in Section 5.4 so that we can obtain a more rigourous and accurate estimation of the SNR. The goal can be simplified by first restricting the input signal to be a single harmonic function. With this simplification, we may be able to directly calculate the Fourier transformation of the amplitude-time function by using Bessel functions. We can also approach the estimation of the SNR of the BIA by proving or disproving that when the maximum amplitude A and the bandwidth W are fixed, the slowest decay rate of $\hat{h}(\xi)$ will be achieved when $f(t) = A sin(Wt)$, which is our current intuition. Another important analysis is the convergence rate of the IASR. As discussed in the last paragraph, we would like to analyze how errors before and after the transformation m_α interacts when measured by the L_2 norm. Another approach for analyzing the convergence rate of the IASR is to restrict the error to be a single harmonic function (i.e. $f_k - f_{k-1} = a \sin bt$) and understand how this error will change after one more iteration.

Another interesting research direction is to understand how we can correct α when the parameter α in the transformation m_α is not precise or is unknown. As mentioned in Section 3.2.3, the function space defined by the scaled amplitude-time functions is invariant under the scaled $\tilde{m}_\alpha$ transformation. With this observation, we may be able to develop algorithms that can correct an inaccurate α by operating more amplitude-time transformations. An interesting observation related to this is that when the amplitude-time function is fixed, only $m_{\frac{1}{\alpha}}$ can transform the function back to a bandlimited function. All the other transformation m_β where $\beta \neq \frac{1}{\alpha}$ will transform the amplitude-time function into a non-bandlimited signal. It is therefore likely to utilize this observation to develop an algorithm.

Other future directions include the generalization of the matrix representation of m_α into, for example, a 3×3 matrix, whether to keep the assumption that f is bandlimited or if we can find a better signal space that can provide us more nice properties for amplitude sampling, and defining other sampling methods that also recover the original function from a timing sequence by defining other transformations.

Bibliography

[1] C. E. Shannon, "Communication in the presence of noise," *Proc. IRE*, vol. 37, pp. 10–21, 1949.

[2] A. D. Wyner and S. Shamai, "Introduction to 'communication in the presence of noise' by c. e. shannon," *Proc. IEEE*, vol. 86, pp. 442–226, Feb. 1998.

[3] M. Unser, "Sampling-50 years after shannon," *Proc. IEEE*, vol. 88, no. 4, pp. 569–587, Apr. 2000.

[4] J. L. Yen, "On nonuniform sampling of bandwidth-limited signals," *Circuit Theory, IRE Transactions on*, vol. 3, no. 4, pp. 251–257, Dec. 1956.

[5] J. W. Mark and T. D. Todd, "A nonuniform sampling approach to data compression," *IEEE Trans. Commun.*, vol. 29, no. 1, pp. 24–32, 1981.

[6] J. B. F. Logan, "Information in the zero crossings of bandpass signals," *AT&T Technical Journal*, vol. 56, pp. 487–510, Apr. 1977.

[7] P. T. Boufounos and R. G. Baraniuk, "Reconstructing sparse signals from their zero crossings," in *Acoustics, Speech and Signal Processing, 2008. ICASSP 2008. IEEE International Conference on*, Mar. 2008, pp. 3361–3364.

[8] H. V. S. N. Sayiner and T. R. Viswanathan, "A level-crossing sampling scheme for a/d conversion," *IEEE Trans. Circuits Syst. II, Analog Digit. Signal Process.*, vol. 43, no. 4, pp. 335–339, Apr. 1996.

[9] L. F. E. Allier, G. Sicard and M. Renaudin, "A new class of asynchronous a/d converters based on time quantization," *Proc. 9th IEEE Int. Symp. Asynchronous Circuits Syst.*, pp. 196–205, 2003.

[10] B. Schell and Y. Tsividis, "A continuous-time adc/dsp/dac system with no clock and with activity-dependent power dissipation," *IEEE J. Solid-State Circuits*, vol. 43, no. 11, pp. 2472–2481, Nov. 2008.

[11] P. Martnez-Nuevo, "Amplitude sampling," *RQE report, MIT*, Nov. 2015.

[12] K. G. H. G. Feichtinger, "Theory and practice of irregular sampling," *Wavelets: mathematics and applications*, pp. 305–363, 1994.

[13] S. M. Nikolskii, *Approximation of Functions of Several Variables and Imbedding Theorems.*   Springer, 1975.

[14] e. Hazewinkel, Michiel, "Composite function," *Encyclopedia of Mathematics.*

[15] A. J. Jerri, "The shannon sampling theoremits various extensions and applications: A tutorial review," *Proceedings of the IEEE*, vol. 65, no. 11, pp. 1565–1596, Nov. 1977.

[16] Y. C. Eldar, *Sampling Theory: Beyond Bandlimited Systems.*   Cambridge University Press, 2015.

[17] H. J. Landau, "Sampling, data transmission, and the nyquist rate," *Proceedings of the IEEE*, vol. 55, no. 10, pp. 1701–1706, Oct. 1967.

[18] A. S. Bandeira, "Sampling and interpolation," *Relax and Conquer*, Sep. 20th 2010.

[19] H. S. Black, *Modulation Theory.*   New York: van Nostrand, 1953.

[20] F. Marvasti, *Nonuniform Sampling - Theory and Practice.*   Kluwer Academic/ Plenum Publishers, 2001.

[21] F. J. Beutler, "Error free recovery of signals from irregular samples," *SIAM Rev.*, pp. 8:322–335, July 1966.

[22] H. J. Landau, "Necessary density conditions for sampling and interpolation of certain entire functions," *Acta Mathematica*, vol. 117, no. 1, p. 37, 1967.

[23] J. N. L. Carleson, P. Malliavan and J. Wermer, *The collected works of Arne Beurling.*   Birkhauser, 1989.

[24] B. Sankur and L. Gerhardt, "Reconstruction of signals from nonuniform samples," *IEEE Int. Conf. Commum., Conf. Rec.*, pp. 15.13–15.18, June 1973.

[25] K. Yao and J. B. Thomas, "On a class of nonuniform sampling representation," *Symp. Signal Trans. Processing*, pp. 69–75, May 1968.

[26] K. Yao and J. B. Thomas, "On some stability and interpolatory properties of nonuniform sampling expansions," *IEEE Transactions on Circuit Theory*, vol. 14, no. 4, pp. 404–408, Dec. 1967.

[27] A. Granas and J. Dugundji, *Fixed Point Theory.*   New York: Springer, 2003.

[28] R. R. Coifman and R. Rochberg, *Representation theorems for holomorfic and harmonic functions in L^p.*   Asterisque 77, 1980.

[29] K. Grochenig, *Describing functions: atomic decompositions versus frames.* Monatsh. Math, 1991.

[30] F. S. A. Quarteroni and P. Gervasio, "Scientific computing with matlab and octave," *Springer*, 2010.

[31] H. Jeffreys and B. S. Jeffreys, *Methods of Mathematical Physics, 3rd ed.*, 1988.

[32] L. N. Trefethen, *Finite Difference and Spectral Methods for Ordinary and Partial Differential Equations.* available at http://people.maths.ox.ac.uk/trefethen/pdetext.html: unpublished text, 1996.

[33] S. Lang, *Complex Analysis.* Springer, 1999.

[34] G. Plya, "On an integral function of an integral function," *Journal London Mathematical Society*, vol. 1, pp. 12–15, 1926.

[35] e. Hazewinkel, Michiel, "Cauchy theorem," *Encyclopedia of Mathematics.*